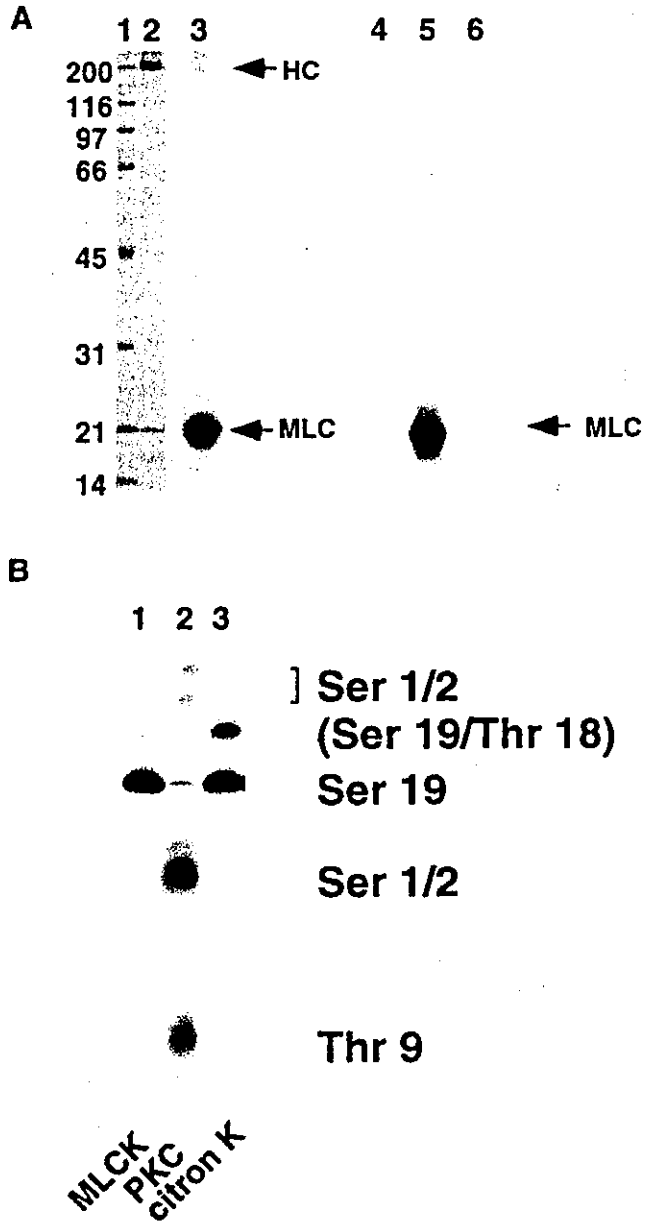

Figure 2. Phosphorylation of RMLC by citron-kinase in vitro. (A) Phosphorylation of MLC by citron-kinase. Citron kinase Δ1 mutant was expressed in COS7 cells, immunoprecipitated with an antimyc antibody, and assayed for phosphorylation using bovine lung myosin II (lanes 2 and 3) or isolated MLC (lanes 4–6) as a substrate. Lanes 1 and 2, Coomassie blue staining. Lane 1, molecular mass markers (numbers in kilodaltons); lane 2, lung myosin plus immunoprecipitated kinase; lane 3, autoradiograph of lane 2. Lanes 4–6, autoradiograph; lane 4, immunoprecipitates from mock-transfected cells; lane 5, immunoprecipitates of citron kinase; lane 6, immunoprecipitates of kinase-defective citron kinase. HC, heavy chain of myosin II; MLC, myosin light chain. (B) One-dimensional phosphopeptide map. Citron kinase phosphorylated both Ser19 and Thr18. Note that citron kinase produced di-phosphorylated MLC to a higher extent than did MLCK. Protein kinase C phosphorylated Ser1/2 and Thr9.

and a mixture of leupeptin, pepstastin, and chymostatin (10 μg/ml each). Cells were homogenized with a Dounce homogenizer and clarified by centrifugation at 16,000 × *g* for 15 min. The supernatant was incubated with a myc mAb (10 μg/100-mm dish) for 1–2 h at 4°C. The immunocomplex was precipitated with protein A-Sepharose (Pharmacia Biotech, Inc., Piscataway, NJ) during a 1-h incubation. The immunocomplex was washed three times with the immunoprecipitation buffer, washed three times with a buffer containing 20 mM Tris-HCl (pH 7.5), 50 mM NaCl, and 5 mM $MgCl_2$, and used for kinase assay.

Phosphorylation Assay

The kinase assays were performed in 25 mM Tris-HCl buffer (pH 7.5) containing 50 mM NaCl, 1 mM DTT, 5 mM $MgCl_2$, 0.1 mM ATP (0.1 mCi/ml), 0.1 mM EGTA, enzyme, and varying amounts of MLC or bovine lung myosin II. Kinases used include immunoprecipitated citron kinase and ROCK, purified MLCK, and Baculovirus-expressed full-length citron kinase. The reaction was performed at 30°C for 3–60 min and terminated by the addition of 2× SDS sample buffer. After SDS-PAGE, MLC bands were cut out and counted by the Cerenkov method. Urea/glycerol gel electrophoresis revealed that purified myosin II was not phosphorylated (our unpublished results).

We also used mono-phosphorylated myosin II as a substrate and prepared it as follows: Purified myosin II was incubated with MLCK (5 μg/ml) in 25 mM Tris-HCl buffer (pH 7.5) containing 50 mM NaCl, 1 mM DTT, 5 mM $MgCl_2$, 0.1 mM $CaCl_2$, 1 mM ATP, and calmodulin (5 μg/ml) at room temperature for 30 min. Phosphorylated myosin II was precipitated by overnight dialysis against 20 mM imidazole buffer (pH 6.5) containing 30 mM KCl and 5 mM $MgCl_2$, washed once with the same buffer, and dissolved in 25 mM Tris-HCl (pH 7.5) containing 0.3 M NaCl. Urea/glycerol gel electrophoresis revealed that more than 90% of myosin II was monophosphorylated under these conditions. To compare the specificity of a substrate between mono-phosphorylated and unphosphorylated myosin II, unphosphorylated myosin II was prepared in the same way as described above except that ATP was omitted when myosin II was phosphorylated with MLCK.

Immunofluorescence

Immunofluorescence was performed using formaldehyde fixation as described (Yamashiro *et al.*, 1998). Exogenously expressed citron kinase or ROCK was detected by immunofluorescence using antimyc mAb or antimyc polyclonal antibody. Changes in phosphorylation of MLC was examined by immunofluorescence using the polyclonal or monoclonal antibodies against mono-phosphorylated MLC or the polyclonal antibody against di-phosphorylated MLC, as described previously (Totsukawa *et al.*, 2000). F-actin was visualized using fluorescently labeled phalloidin (Sigma). Cells were examined with a Nikon TE 300 inverted microscope. Phase and fluorescence images were taken with a Photometric CoolSnap-fx CCD camera (Roper Scientific Inc., Tucson, AZ) and processed with IPLab image processing software (Scanalytics, Inc., Fairfax, VA).

Other Procedures

SDS-PAGE was performed as described (Blatter *et al.*, 1972) using 12.5% polyacrylamide except that the buffer system of Laemmli (1970) was used. Protein concentrations were determined using an Advanced Protein Assay reagent (Cytoskeleton, Denver, CO) with bovine serum albumin as a standard. Phosphopeptide mapping of phosphorylated MLC was performed as described (Yamakita *et al.*, 1994).

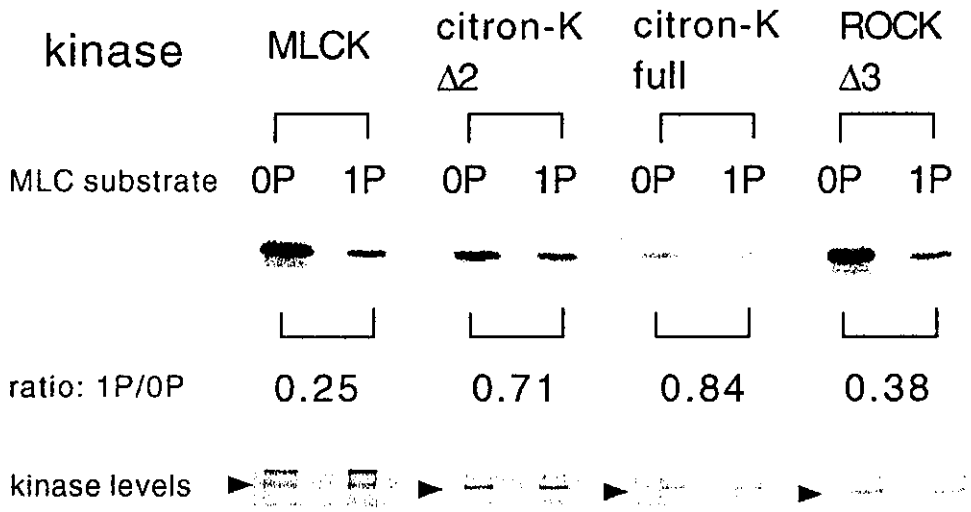

Figure 3. Citron kinase phosphorylates mono-phosphorylated MLC as well as it does un-phosphorylated MLC. MLC kinase reactions were performed using either unphosphorylated myosin (0P) or mono-phosphorylated myosin (1P) as a substrate. Myc-tagged, full-length citron kinase, Δ2 citron kinase, or Δ3 ROCK was expressed in COS7 cells, immunoprecipitated by a myc antibody, and used for kinase reactions. Purified MLCK was also used. Ratios of phosphate incorporation between mono-phosphorylated MLC and unphosphorylated MLC are shown. Kinase levels are shown in the bottom panel (Coomassie blue staining). The results are representative of three independent experiments.

RESULTS

Phosphorylation of Regulatory Light Chain (MLC) of Myosin II by Citron Kinase In Vitro

We found that citron kinase phosphorylated MLC in vitro. A Δ1deletion mutant (that contains the N-terminus kinase domain as well as the coiled-coil and the Rho binding domain; Madaule *et al.*, 1998) of myc-tagged citron kinase was expressed in COS7 cells, immunoprecipitated by an antimyc antibody, and used for kinase assay using bovine lung myosin II as a substrate. As Figure 2A shows, immunoprecipitated citron kinase was able to phosphorylate MLC of intact myosin II (lanes 2 and 3). It also phosphorylated isolated MLC (lane 5). As a control, a kinase defective (KD) mutant of citron kinase was immunoprecipitated in the same way and used for its kinase activity. The KD mutant failed to phosphorylate MLC (lane 6). In addition, immunoprecipitates from MOCK-transfected cells did not phosphorylate MLC (lane 4). These results suggest that citron kinase itself, rather than an unknown kinase associated or contaminated with immunoprecipitated citron kinase, phosphorylates MLC. We examined other constructs of citron kinase including mutants with further deletion of the C terminus (Δ2, the kinase domain plus half of the coiled-coil domain, and Δ3, kinase domain alone) as well as full-length citron kinase, which all phosphorylated MLC. As the Δ3 mutant consists of the kinase domain alone, it is unlikely that an unknown kinase associated with this mutant phosphorylates MLC.

The sites of MLC phosphorylated by citron kinase were identified by one-dimensional phosphopeptide mapping (Yamakita *et al.*, 1994). As Figure 2B shows, citron kinase generated two phosphopeptides, one corresponding to a peptide phosphorylated at Ser19 and the other to a peptide phosphorylated at both Ser19 and Thr 18 (lane 3). As a control, phosphopeptide patterns of MLC phosphorylated by MLCK or PKC are shown in lanes 1 and 2, respectively. It should be noted that citron kinase produced di-phosphorylated MLC to a higher extent than did MLCK.

It is possible that citron kinase phosphorylates mono-phosphorylated MLC as well as it does unphosphorylated MLC, thus generating more di-phosphorylated MLC than did MLCK. We thus measured activities of citron kinase, ROCK, and MLCK using both unphosphorylated (0P) and mono-phosphorylated (1P) myosin II as a substrate. As Figure 3 shows, both full-length and mutant citron kinases phosphorylated these two substrates equally well. In contrast, MLCK or ROCK phosphorylated un-phosphorylated MLC much better than they did mono-phosphorylated MLC. The ratios of phosphate incorporation between unphosphorylated and mono-phosphorylated substrate are 0.7–0.8 for citron kinase, 0.2–0.3 for MLCK, and 0.3–0.4 for ROCK.

Citron Kinase Does Not Phosphorylate MBS of Myosin Phosphatase

It is well known that ROCK phosphorylates MBS of myosin phosphatase. Because the kinase domain of ROCK shows 46% identity to that of citron kinase (Madaule *et al.*, 1998), we examined whether citron kinase was able to phosphorylate MBS. The kinase domain of myc-tagged ROCK or citron kinase was expressed in COS7 cells, immunoprecipitated, and assayed for their kinase activities using both MLC and MBS as a substrate (Figure 4). As Figure 4a shows, phosphorylation of MBS by citron kinase (lane 2) was as low as that of mock transfection (lane 1). On the other hand, ROCK phosphorylated MBS (lane 3). The lack of phosphate incorporation into the MBS by citron kinase is neither due to inactive kinase activity of immunoprecipitated citron kinase nor poor expression of citron kinase. Both citron kinase and ROCK phosphorylated MLC to a similar extent (lanes 2 and 3 of Figure 4b). In addition, Western blotting with a myc antibody (c) revealed that the expression level of citron kinase (lane 2) in COS7 cells was ~5 times higher than that of ROCK (lane 3). These results indicate that the activity of citron kinase toward MBS is insignificant.

Kinetic Analysis of Citron Kinase

To estimate the molecular activity and K_m of citron kinase, full-length citron kinase complexed with constitutively ac-

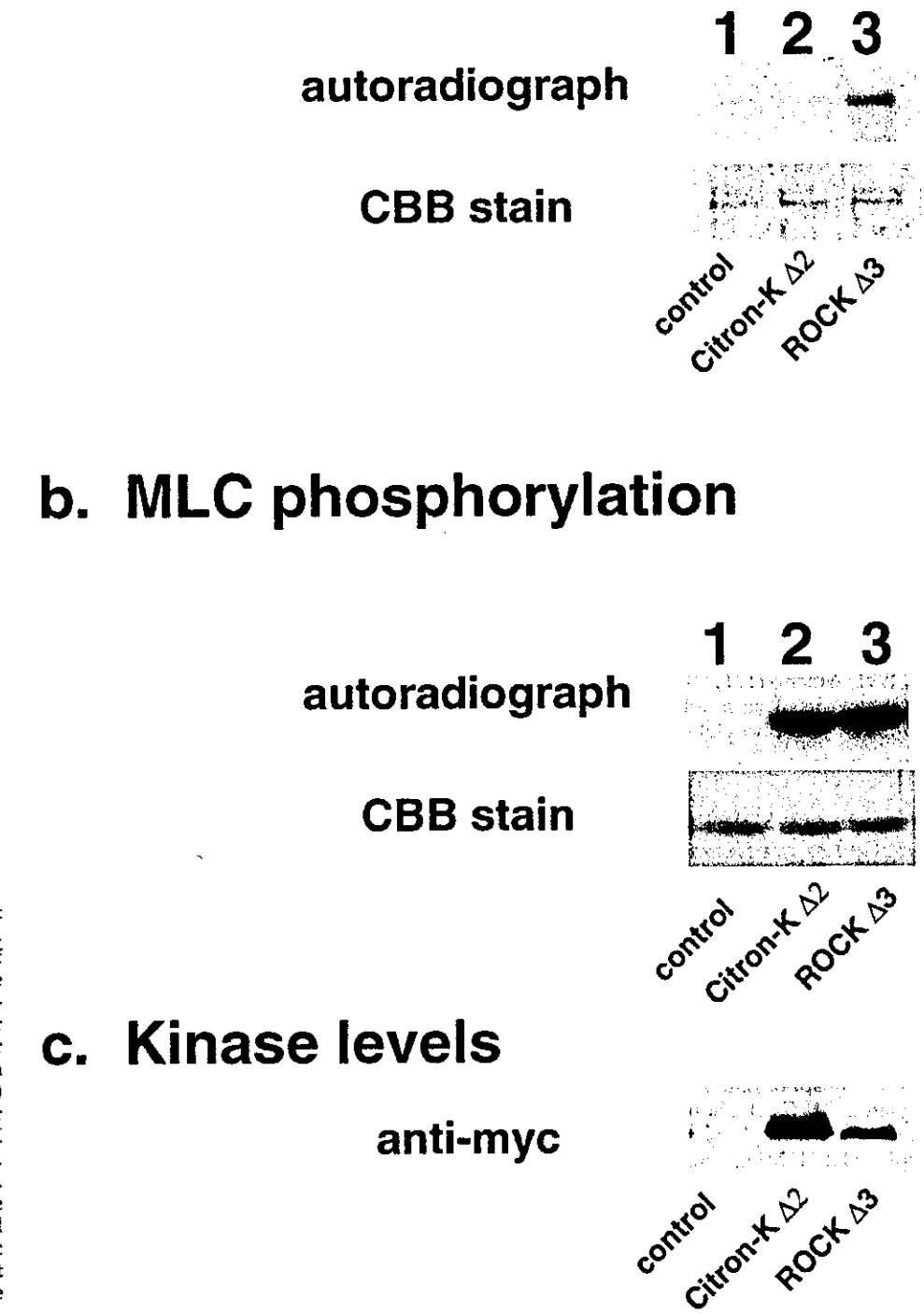

Figure 4. Citron kinase does not significantly phosphorylate MBS. The kinase domain mutants (Δ2) of citron kinase and ROCK (Δ3) were expressed in COS7 cells, immunoprecipitated, and assayed for their kinase activities using MBS (a) or MLC (b) as a substrate. Both citron kinase (lane 2) and ROCK (lane 3) phosphorylated MLC to a similar extent (b). However, only ROCK phosphorylated MBS (lane 3 of a). Lane 1 is control without kinase. The levels of kinase used are shown in c, which were detected by immunoblot using the antimyc antibody. CBB, Coomassie brilliant blue. The results are representative of three independent experiments.

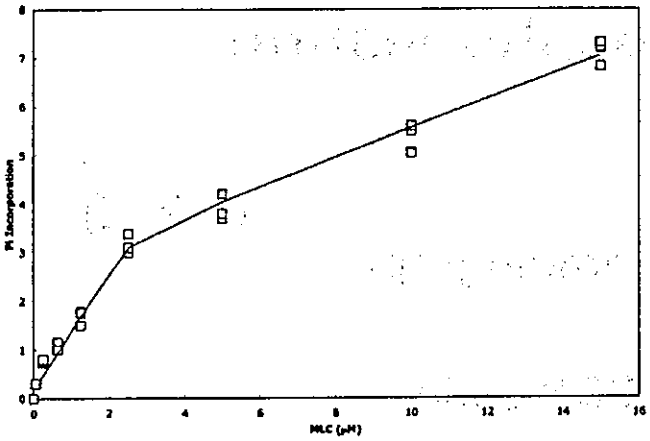

Figure 5. Phosphorylation of MLC by Baculovirus-expressed full-length citron kinase. Full-length citron kinase (5 ng/μl) was incubated at 30°C for 5 min with varying concentrations (0.25–15 μM) of MLC. Pi incorporation is in pmol.

tive GST-RhoA was used for phosphorylation with varying concentrations of MLC (Figure 5). The apparent K_m and molecular activity of full-length citron kinase were 6.6 ± 1.0 μM and 0.3 ± 0.09 s^{-1}, respectively. The K_m value is comparable to the values (0.9–2.5 μM) reported for Rho-kinase and those (5–52 μM) of MLCK (Adelstein and Klee, 1981b; Gallagher *et al.*, 1991; Amano *et al.*, 1996; Feng *et al.*, 1999). On the other hand, the molecular activity of citron kinase is lower than the values reported for Rho-kinase (0.67–2 s^{-1}) and MLCK (2–65 s^{-1}; Adelstein and Klee, 1981b; Gallagher *et al.*, 1991; Amano *et al.*, 1996; Feng *et al.*, 1999). When intact myosin was used as a substrate, full-length citron kinase was able to phosphorylate MLC up to 0.5–0.7 mol/mol of MLC.

Increase in MLC Di-phosphorylation by the Expression of the Kinase Domain of Citron Kinase in Cultured Cells

To further test whether citron kinase phosphorylates MLC, cultured cells were transfected with myc-tagged citron kinase and stained with the phospho-MLC specific antibodies. Immunofluorescence with the phospho-MLC specific antibodies has allowed us to determine changes in MLC phosphorylation in transfected cells (detected by a myc antibody; Totsukawa *et al.*, 2000). We used two antibodies, one specific to mono-phosphorylated MLC and the other to di-phosphorylated MLC. It should be noted that the antibody against mono-phosphorylated MLC did not recognize di-phosphorylated MLC and the antibody against di-phosphorylated MLC did not recognize mono-phosphorylated MLC. Actin organization was also examined by phalloidin staining.

We examined the effects of the Δ2 mutant of citron kinase on MLC phosphorylation of PTK cells (Figure 6). This mutant, which consists of the kinase domain and a part of the coiled-coil domain (see Figure 1), distributed diffusely throughout the cytoplasm (asterisk in A, D, and G; Eda *et al.*, 2001). Surprisingly, when transfected cells were stained with the antibody specific to mono-phosphorylated MLC, they showed lower staining (asterisk in B). Quantitative measurement showed that staining intensity with the mono-phosphorylated antibody was reduced to 45 ± 25% of the control (n = 30). However, phalloidin staining revealed that transfected cells retained well-developed stress fibers (asterisk in C). Because stress fiber formation depends on actomyosin contractility and MLC phosphorylation (Chrzanowska-Wodnicka and Burridge, 1996; Totsukawa *et al.*, 2000) and because citron kinase produced di-phosphorylated MLC in vitro, we thought myosin may be di-phosphorylated. Indeed, transfected cells (asterisks in E) exhibited significantly higher staining with the antibody specific to di-phosphorylated MLC, indicating that di-phosphorylation was increased. Again phalloidin staining (F) revealed that transfected cells had well-developed stress fibers. To confirm the changes in MLC phosphorylation, transfected cells were triple-labeled with the antibodies against myc (G), mono- (H), and di-phosphorylated MLC (I). The increase in di-phosphorylation (I) with simultaneous decrease in mono-phosphorylation (H) was clearly seen in transfected cells (asterisks in G). A similar result was obtained with Δ3 mutant of citron kinase (which contains the kinase domain alone). These observations indicate that the expression of kinase domain of citron kinase caused an increase in MLC di-phosphorylation.

The increase in di-phosphorylation becomes more evident when ROCK activity is blocked by a specific inhibitor, Y-27632. The inhibition of ROCK is known to result in the disassembly of stress fibers (Ishizaki *et al.*, 2000). As Figure 6, J–L shows, however, cells expressing Δ2 citron kinase (asterisks in J) retained well-developed stress fibers (asterisks in L). At the same time, these transfected cells clearly exhibited an increase in MLC di-phosphorylation (asterisks in K), indicating that di-phosphorylation efficiently restores the assembly of stress fibers. In contrast, surrounding cells expressing no citron kinase lost staining with the antibody against di-phosphorylated MLC (K), and stress fibers of these nontransfected cells were disassembled (L). These results indicate that citron kinase is able to generate di-phosphorylation of MLC even when myosin phosphatase is activated by the inhibition of ROCK.

To compare the effects of citron kinase with those of ROCK, we examined how the expression of the kinase domain of ROCK (Δ3 mutant) alters MLC phosphorylation (Figure 7). As revealed by phalloidin staining (C and F), expression of ROCK frequently induced the formation of characteristic stellar stress fibers (C), which is consistent with the previous reports (Leung *et al.*, 1996; Amano *et al.*, 1997; Ishizaki *et al.*, 1997). These stellar stress fibers were highly stained with the antibodies against either mono- (B) or di-phosphorylated MLC (E). The increase in both mono- and di-phosphorylation of MLC by ROCK overexpression is probably due to the two activities of ROCK: ROCK can directly phosphorylate MLC (Amano *et al.*, 1996; Totsukawa *et al.*, 2000) and at the same time inhibit myosin phosphatase (Kimura *et al.*, 1996).

The changes in MLC phosphorylation by citron kinase or by ROCK were confirmed biochemically using Western blotting (Figure 8). BHK cells were used for this purpose because they are more efficient for transfection. Cells were transfected with either citron kinase Δ2 mutant or ROCK Δ3

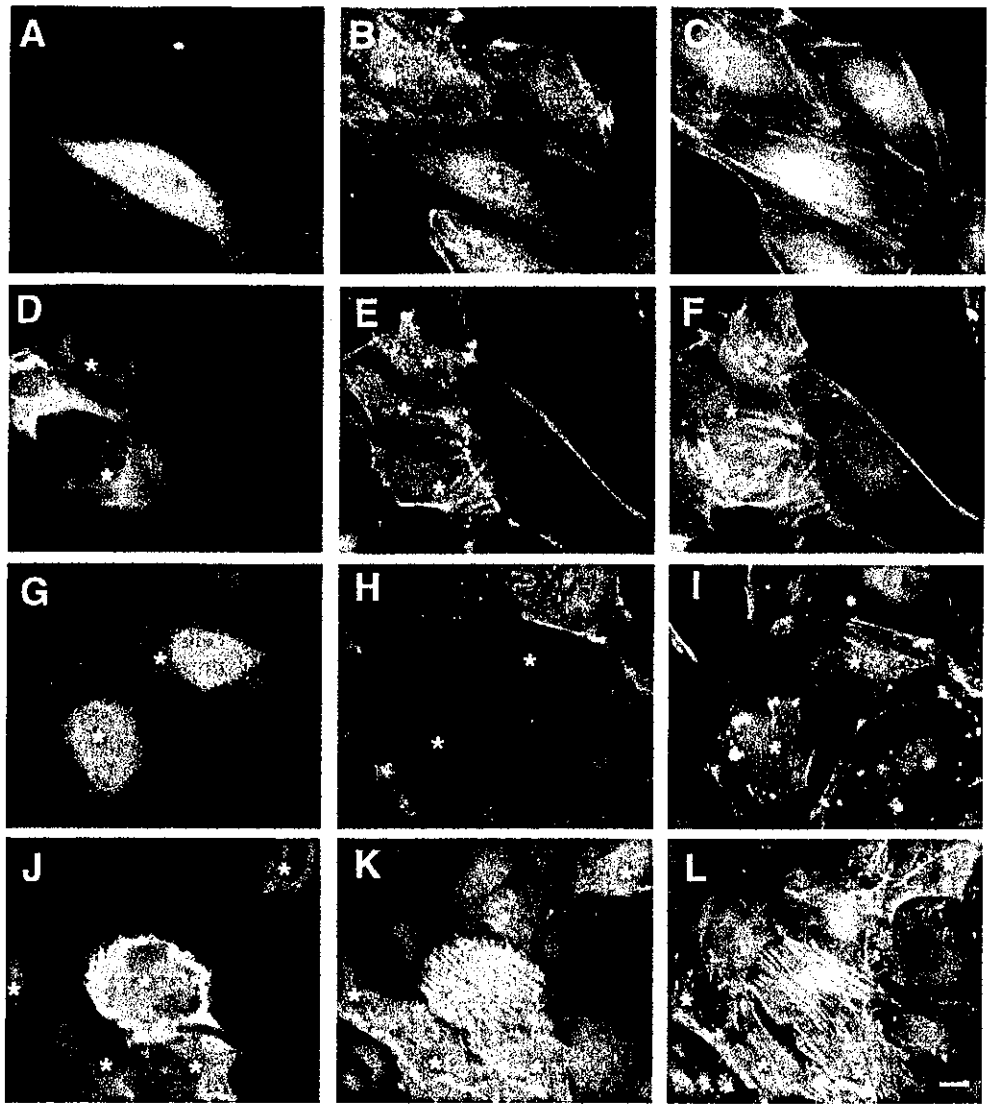

Figure 6. Di-phosphorylation of MLC in vivo by citron kinase. PTK cells were first transfected with Δ2 citron kinase and then immunolabeled with the specific antibodies against myc (A, D, G, and J), against mono-phosphorylated MLC (B and H), and against di-phosphorylated MLC (E, I, and K). F-actin was also visualized by labeling with fluorescent phalloidin (C, F, and L). Asterisks indicate cells expressing myc-tagged mutant citron kinase. Cells in J–L were treated with a specific inhibitor of ROCK, Y-27632, for 30 min before immunofluorescence staining. The expression of Δ2 citron kinase increased di-phosphorylation of MLC (asterisks in E, I, and K) but decreased mono-phosphorylation (asterisk in B and H). Bar, 10 μm.

mutant. Total cell lysates were then immunoblotted using the antibodies specific to mono- or di-phosphorylated MLC (middle panels) as well as the myc antibody to detect levels of expression (top panels). Similar amounts of lysates were loaded for each lane (bottom panels). Cells transfected with citron kinase showed lower reactivity to the antibody against mono-phosphorylated MLC (lane 2 of Figure 8a) than did mock-transfected cells (lane 1). On the other hand, the immunoblot with the antibody against di-phosphorylated MLC revealed higher reactivity with citron kinase-transfected cells (lane 2 of Figure 8b) than with mock-transfected cells (lane 1). ROCK-transfection increased both mono- and di-phosphorylation of MLC to a great extent (lane 3 of Figure 8, a and b, respectively), which is probably due to the inhibition of myosin phosphatase by ROCK. These data are consistent with the immunofluorescence observations (Figures 6 and 7).

We then examined whether the expression of full-length citron kinase alters MLC phosphorylation. Previous work has demonstrated that, although full-length citron kinase is present as protein aggregates in interphase cells, it becomes dispersed during prophase and localized in cleavage furrows during cytokinesis (Eda *et al.*, 2001). Because RhoA is likely to activate citron kinase during cytokinesis, we examined whether the expression of full-length citron kinase alters MLC di-phosphorylation during cytokinesis. To this end, we chose CHO cells because CHO cells are relatively easily synchronized and show good transfection efficiency. As Figure 9 shows, we have expressed GFP-tagged full-length citron kinase in synchronized CHO cells (A) and stained them with the antibody against di-phosphorylated MLC (B) and DAPI (C). As a control, GFP alone was expressed (D) and stained with the anti-di-phosphorylated MLC antibody (E) and DAPI (F). GFP-citron kinase was localized in cleavage furrows (A) where strong staining of MLC di-phosphorylation was observed (B). Quantitative analyses of immunofluorescence revealed that staining intensities of di-phosphorylation more than doubled. On the

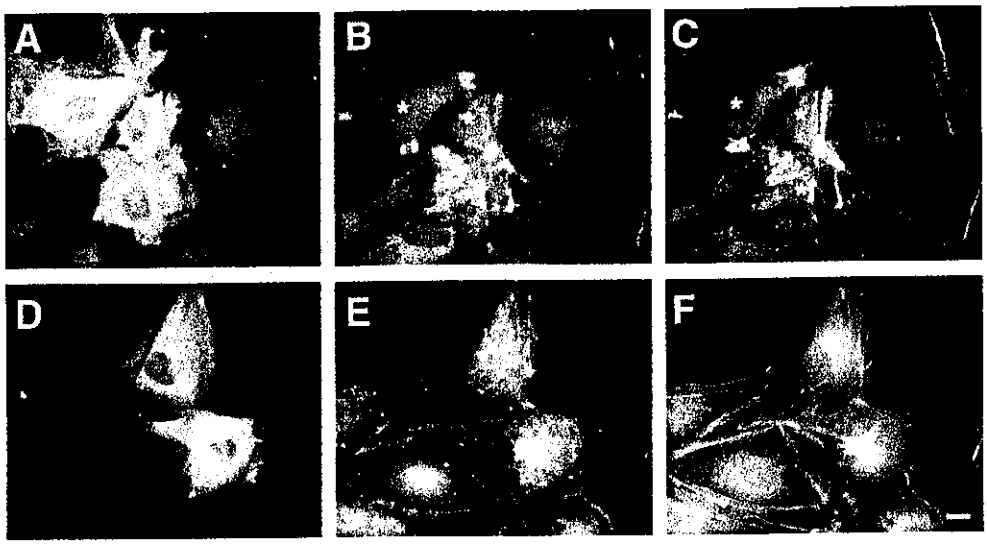

Figure 7. Increases in mono- and di-phosphorylation by the expression of ROCK. PTK cells were transfected with Δ3 mutant of ROCK (equivalent to Δ2 mutant of citron kinase) and then stained with antimyc (A and D), anti–mono-phosphorylated MLC (B), and anti–di-phosphorylated MLC (E) antibodies. F-actin structure was visualized by labeling with fluorescent phalloidin (C and F). Cells expressing myc-tagged mutant ROCK are indicated by asterisks. Note that ROCK increases both mono- and di-phosphorylation of MLC. Stellar stress fibers were frequently formed. Bar, 10 μm.

other hand, control cells expressing GFP alone (D) showed di-phosphorylation indistinguishable from untransfected cells (E).

In interphase cells, GFP-tagged citron kinase showed punctate localization, as reported previously (Madaule *et al.*, 1998; Eda *et al.*, 2001). Such cells showed no changes in MLC mono- or di-phosphorylation (our unpublished results). This lack of effects is likely due to the fact that the localization of full-length citron kinase is constrained to protein aggregates (Eda *et al.*, 2001), which would restrict the access of the kinase to a substrate.

Localization of Mono- and Di-phosphorylated MLC during Cell Division

We examined the localization of di-phosphorylated MLC during cell division. Figure 10 shows double-labeled immunofluorescence localization of both mono-phosphorylated (A, D, and G) and di-phosphorylated (B, E, and H) MLC in NRK cells at different stages of cytokinesis. From metaphase (our unpublished results) to early anaphase (A–C), both mono- and di-phosphorylated MLC showed diffuse staining though anti–di-phosphorylated MLC antibody stained centrioles. At telophase (D–F), both mono- (D) and di-phosphorylated (E) MLC colocalized at cleavage furrows. It is interesting to note that di-phosphorylated MLC showed more constrained localization in cleavage furrows than did mono-phosphorylated MLC. At late telophase (G and H), the constrained localization of di-phosphorylated MLC became clearer.

DISCUSSION

We have shown here that citron kinase, like ROCK, is able to function as an MLC kinase. In vitro, citron kinase phosphor-

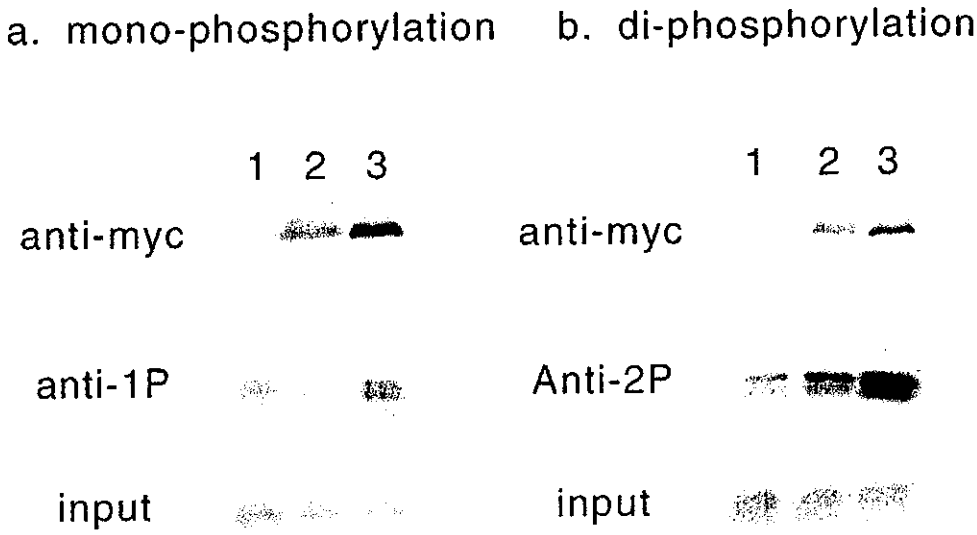

Figure 8. Increase in di-phosphorylation and decrease in mono-phosphorylation of MLC by expression of citron kinase. BHK cells were first transfected with Δ2 mutant of citron kinase or Δ3 mutant of ROCK, then total cell lysates were immunoblotted with antibodies against mono-phosphorylated MLC (middle panel of a) or against di-phosphorylated MLC (middle panel of b). Lane 1, mock-transfection; lane 2, transfection with Δ 2 citron kinase mutant; lane 3, transfection with Δ3 ROCK mutant. The same lysates were also immunoblotted with antimyc antibody to show levels of expression (top panels). Coomassie blue staining of histone H3 of total cell lysates are shown in the lower panels to indicate the loading.

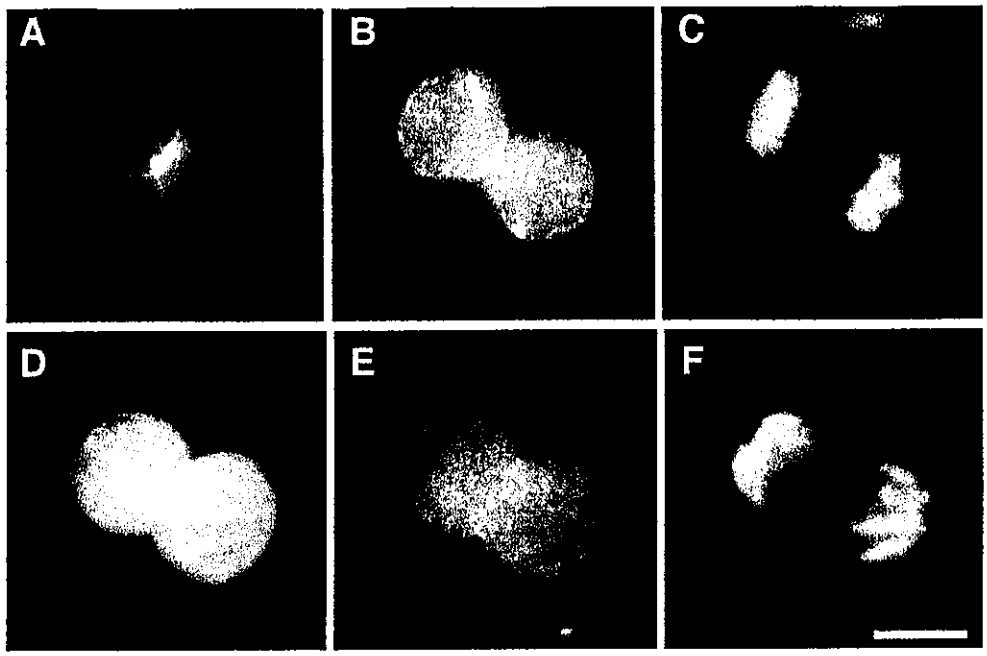

Figure 9. Di-phosphorylation of MLC during cytokinesis by the expression of full-length citron kinase. CHO cells were transfected with GFP-full-length citron kinase (A–C) or GFP alone (D–F) and synchronized for cell division. A and D, GFP. Cleaving cells were labeled with the anti–di-phosphorylated MLC antibody (B and E) and with DAPI (C and F).

ylates MLC at both Ser19 and Thr18. The expression of the kinase domain causes di-phosphorylation of MLC in a variety of cells. To our knowledge, MLC is the first physiological substrate of citron kinase. Because citron kinase is localized in cleavage furrows (Madaule *et al.*, 1998; Kosako *et al.*, 1999; Kosako *et al.*, 2000; Fukata *et al.*, 2001), it is likely to activate myosin during cytokinesis. The presence of the two RhoA-activated MLC kinases, citron kinase and ROCK, in cleavage furrows may explain why the ROCK inhibitor, Y-27632, does not effectively inhibit cytokinesis (Madaule *et al.*, 2000). The direct phosphorylation of MLC by citron kinase may also account for abnormal contractility of "push and pull" movements during cytokinesis when a kinase active mutant of citron kinase is overexpressed (Madaule *et al.*, 2000).

Although both ROCK and citron kinase phosphorylate MLC, there are two important differences in their activities. First, citron kinase does not phosphorylate MBS of myosin phosphatase (Figure 4) and thus does not inhibit myosin phosphatase activity. In contrast, ROCK phosphorylates MBS, inhibiting the activity of myosin phosphatase. This indicates that ROCK would block the turnover of MLC phosphorylation, making most MLC to be the phosphorylated form of MLC. Both immunofluorescence (Figure 6) and biochemical analysis (Figure 8) support this notion. When constitutively active ROCK is expressed in cells, stellar actin fibers are assembled (Figure 7), which is likely to be a result of contraction of actomyosin due to a very high extent of MLC phosphorylation (Figure 8). In contrast, citron kinase would not block turnover of MLC phosphorylation. Consistent with this notion, cells expressing the kinase domain of citron kinase exhibit parallel stress fibers with apparently normal morphology (Figure 6).

Second, the expression of citron kinase in cells resulted in an increase in di-phosphorylation of MLC but a decrease in MLC mono-phosphorylation (Figure 6). This is in contrast to the expression of ROCK in which both mono- and di-phosphorylation were increased (Figure 7). The increase in di-phosphorylated MLC by the citron kinase domain is apparently explained by the result that citron kinase phosphorylated mono-phosphorylated MLC as well as it did un-phosphorylated MLC (Figure 3). This ability of citron kinase may also explain the decrease in mono-phosphorylation of MLC because citron kinase would effectively convert mono-phosphorylated myosin to di-phosphorylated myosin.

Other interpretations are also possible. For example, citron kinase may activate a myosin phosphatase that is specific for mono-phosphorylated myosin, although no such phosphatase has been known. Another possibility is that citron kinase phosphorylates and inhibits other major MLC kinases. If citron kinase, for example, inhibited MLCK, then mono-phosphorylated MLC may be reduced. We found, however, that citron kinase did not phosphorylate MLCK or ROCK, which are believed to be two major MLC kinases inside cells. Further studies are necessary to determine whether citron kinase modulates other MLC kinases including PAK (Chew *et al.*, 1998; Zeng *et al.*, 2000) and ZIP kinase (Murata-Hori *et al.*, 1999, 2001).

The activity of citron kinase is likely to be regulated in a cell cycle–dependent manner. Citron kinase has been reported to be present as protein aggregates in interphase cells (Eda *et al.*, 2001), and as such, it may not be active. In contrast, ROCK is diffusely localized in interphase cells. ROCK is, at least in part, active as its activity is known to be essential for the formation of stress fibers (Leung *et al.*, 1996; Amano *et al.*, 1997; Ishizaki *et al.*, 1997; Nakano *et al.*, 1999; Watanabe *et al.*, 1999; Totsukawa *et al.*, 2000). During prophase, citron kinase becomes dispersed and is translocated to cleavage furrows during cytokinesis (Eda *et al.*, 2001). Because Rho A has been reported to be greatly activated during cytokinesis (Kimura *et al.*, 2000), citron kinase is likely to become activated. This activation probably accounts, at least in part, for the di-phosphorylation of MLC at

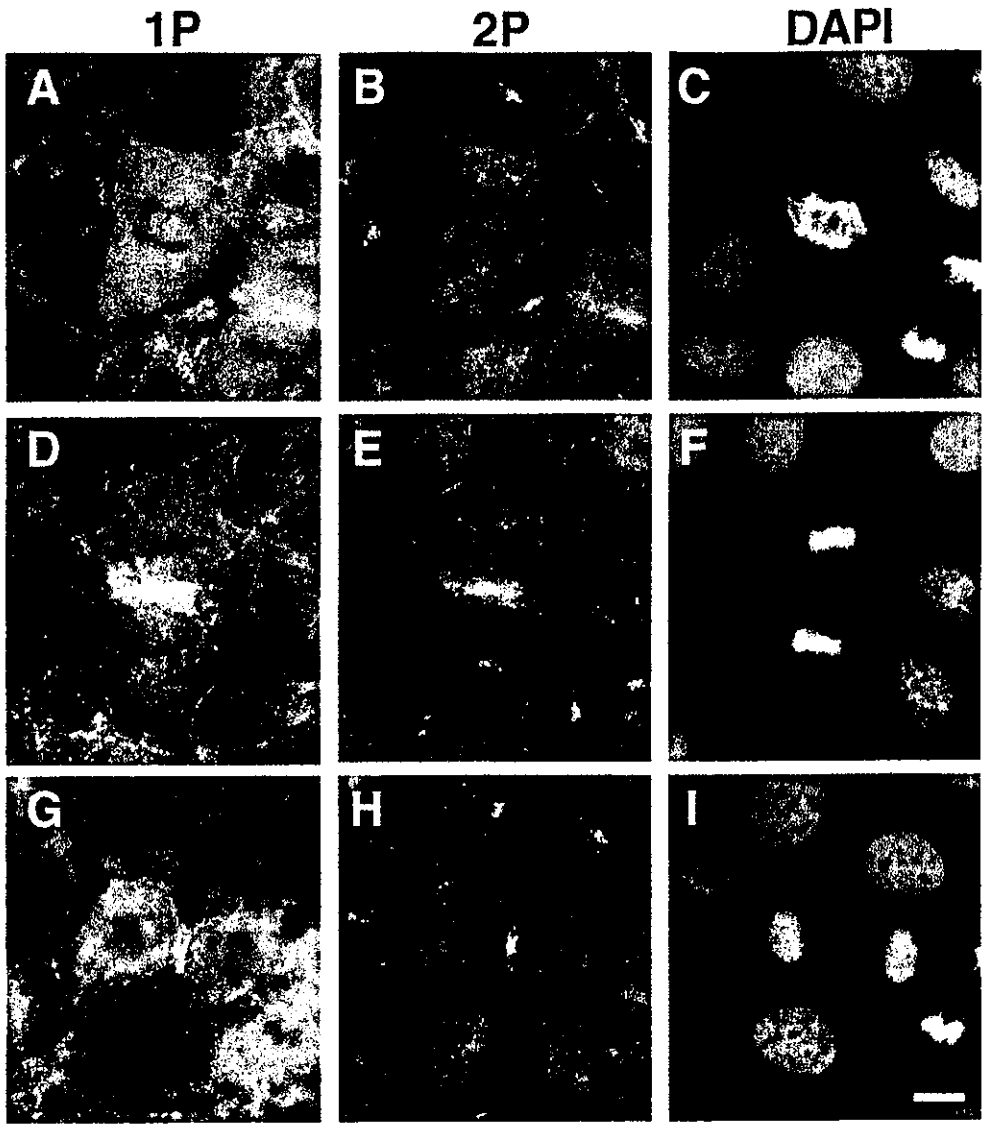

Figure 10. Localization of mono- and di-phosphorylated MLC during cell division. NRK cells at different stages of cell division were stained with the antibodies against mono-phosphorylated MLC (A, D, and G), di-phosphorylated MLC (B, E, and H), and DAPI (C, F, and I). A–C, early anaphase; D–F, telophase; G–I, late telophase. Note that di-phosphorylated MLC in cleavage furrows is more constrained than is mono-phosphorylated MLC. Bar, 10 μm.

cleavage furrows (Figures 9 and 10) although other kinases such as ROCK may also be involved in the di-phosphorylation of MLC.

Di-phosphorylated myosin showed more constrained localization at cleavage furrows than did mono-phosphorylated myosin (Figure 10). Although di-phosphorylated myosin showed twofold higher ATPase activity than mono-phosphorylated myosin (Ikebe and Hartshorne, 1985), the velocity of actin filaments in an in vitro motility assay is the same for both types of phosphorylated myosin (Umemoto *et al.*, 1989). On the other hand, di-phosphorylation significantly increases thick filament assembly and actomyosin superprecipitation (Ikebe and Hartshorne, 1985), suggesting that di-phosphorylated myosin may play a role in cross-linking of actin filaments rather than stimulation of motor activity. Further studies are required to elucidate the exact role of di-phosphorylation of MLC in cleavage furrows.

It now appears that three different kinases including MLCK, ROCK, and citron kinase are all localized in cleavage furrows (Madaule *et al.*, 1998; Kosako *et al.*, 1999, 2000; Poperechnaya *et al.*, 2000; Fukata *et al.*, 2001; Chew *et al.*, 2002) and are functioning as MLC kinases. In addition, MBS of myosin phosphatase phosphorylated by Rho-kinase (ROCK) is also localized in cleavage furrows (Kawano *et al.*, 1999). These results reinforce the importance of the regulation of MLC phosphorylation during cytokinesis. An important question is why citron kinase–deficient mice show a cytokinesis defect in some neuronal precursor cells even though these cells express abundant ROCK (Di Cunto *et al.*, 2000). This observation indicates that citron kinase plays a role distinct from ROCK. As discussed above, citron kinase, unlike ROCK, does not block turnover of MLC phosphorylation while generating di-phosphorylated MLC. This ability of citron kinase to allow turnover may be important for

certain cells to complete cytokinesis. For example, ROCK may be activated by Rho to a much higher extent in the absence of citron kinase than in its presence because Rho may not be shared between ROCK and citron kinase. Such overactivation of ROCK may result in the MLC phosphorylation to a very high extent while blocking dephosphorylation of MLC or turnover of MLC phosphorylation. Blockage of MLC dephosphorylation may hinder the proper execution of cytokinesis because cytokinesis is known to be associated with simultaneous contraction and disassembly of contractile rings, and the disassembly is likely to require MLC dephosphorylation or turnover. It is also quite possible that citron kinase controls cytokinesis by phosphorylating unique substrates that ROCK cannot phosphorylate. Future studies should be directed at elucidating whether citron kinase indeed regulates MLC di-phosphorylation during cytokinesis in a way distinct from ROCK or whether citron kinase has other substrates that are critical in regulating other aspects of cell division.

ACKNOWLEDGMENTS

We thank Yoshitomi Pharmaceutical Industries, Ltd. For providing Y-27632, and Dr. F. Deis (Rutgers) for critical reading of this manuscript. The work is supported by the National Institutes of Health Grant CA42742 (to F.M.), American Heart Association grant (to S.Y.), and the Bush Memorial Fund. F.M. is a member of the Cancer Institute of New Jersey. G.T. is supported by a fellowship from the Leukemia Research Foundation and the American Heart Association.

REFERENCES

Adelstein, R.S., and Klee, C.B. (1981a). Purification and characterization of smooth muscle myosin light chain kinase. J. Biol. Chem. *256*, 7501–7509.

Adelstein, R.S., and Klee, C.B. (1981b). Purification and characterization of smooth muscle myosin light chain kinase. J. Biol. Chem. *256*, 7501–7509.

Alessi, D., MacDougall, L.K., Sola, M.M., Ikebe, M., and Cohen, P. (1992). The control of protein phosphatase-1 by targetting subunits. The major myosin phosphatase in avian smooth muscle is a novel form of protein phosphatase-1. Eur. J. Biochem. *210*, 1023–1035.

Amano, M., Chihara, K., Kimura, K., Fukata, Y., Nakamura, N., Matsuura, Y., and Kaibuchi, K. (1997). Formation of actin stress fibers and focal adhesions enhanced by Rho-kinase. Science *275*, 1308–1311.

Amano, M., Ito, M., Kimura, K., Fukata, Y., Chihara, K., Nakano, T., Matsuura, Y., and Kaibuchi, K. (1996). Phosphorylation and activation of myosin by Rho-associated kinase (Rho-kinase). J. Biol. Chem. *271*, 20246–20249.

Blatter, D.P., Garner, F., Van Slyke, K., and Bradley, A. (1972). Quantitative electrophoresis in polyacrylamide gels of 2–40%. J. Chromatogr. *64*, 147–155.

Bokoch, G.M. (2000). Regulation of cell function by Rho family GTPases. Immunol. Res. *21*, 139–148.

Chew, T.-L., Wolf, W.A., Gallagher, P.J., Matsumura, F., and Chisholm, R.L. (2002). A fluorescent resonant energy transfer-based biosensor reveals transient and regional myosin light chain kinase activation in lamella and cleavage furrows. J. Cell Biol. *156*, 543–553.

Chew, T.L., Masaracchia, R.A., Goeckeler, Z.M., and Wysolmerski, R.B. (1998). Phosphorylation of non-muscle myosin II regulatory light chain by p21-activated kinase (gamma-PAK). J. Muscle Res. Cell Motil. *19*, 839–854.

Chrzanowska-Wodnicka, M., and Burridge, K. (1996). Rho-stimulated contractility drives the formation of stress fibers and focal adhesions. J. Cell Biol. *133*, 1403–1415.

Di Cunto, F., Calautti, E., Hsiao, J., Ong, L., Topley, G., Turco, E., and Dotto, G.P. (1998). Citron rho-interacting kinase, a novel tissue-specific ser/thr kinase encompassing the Rho-Rac-binding protein Citron. J. Biol. Chem. *273*, 29706–29711.

Di Cunto, F. *et al.* (2000). Defective neurogenesis in citron kinase knockout mice by altered cytokinesis and massive apoptosis. Neuron *28*, 115–127.

Eda, M., Yonemura, S., Kato, T., Watanabe, N., Ishizaki, T., Madaule, P., and Narumiya, S. (2001). Rho-dependent transfer of Citron-kinase to the cleavage furrow of dividing cells. J. Cell Sci. *114*, 3273–3284.

Feng, J. *et al.* (1999). Rho-associated kinase of chicken gizzard smooth muscle. J. Biol. Chem. *274*, 3744–3752.

Fukata, Y., Amano, M., and Kaibuchi, K. (2001). Rho-Rho-kinase pathway in smooth muscle contraction and cytoskeletal reorganization of non-muscle cells. Trends Pharmacol. Sci. *22*, 32–39.

Furuyashiki, T., Fujisawa, K., Fujita, A., Madaule, P., Uchino, S., Mishina, M., Bito, H., and Narumiya, S. (1999). Citron, a Rho-target, interacts with PSD-95/SAP-90 at glutamatergic synapses in the thalamus. J. Neurosci. *19*, 109–118.

Gallagher, P.J., Herring, B.P., Griffin, S.A., and Stull, J.T. (1991). Molecular characterization of a mammalian smooth muscle myosin light chain kinase. J. Biol. Chem. *266*, 23936–23944.

Ikebe, M., and Hartshorne, D.J. (1985). Phosphorylation of smooth muscle myosin at two distinct sites by myosin light chain kinase. J. Biol. Chem. *260*, 10027–10031.

Ishizaki, T., Naito, M., Fujisawa, K., Maekawa, M., Watanabe, N., Saito, Y., and Narumiya, S. (1997). p160ROCK, a Rho-associated coiled-coil forming protein kinase, works downstream of Rho and induces focal adhesions. FEBS Lett. *404*, 118–124.

Ishizaki, T., Uehata, M., Tamechika, I., Keel, J., Nonomura, K., Maekawa, M., and Narumiya, S. (2000). Pharmacological properties of Y-27632, a specific inhibitor of rho-associated kinases. Mol. Pharmacol. *57*, 976–983.

Kawano, Y., Fukata, Y., Oshiro, N., Amano, M., Nakamura, T., Ito, M., Matsumura, F., Inagaki, M., and Kaibuchi, K. (1999). Phosphorylation of myosin-binding subunit (MBS) of myosin phosphatase by Rho-kinase in vivo. J. Cell Biol. *147*, 1023–1038.

Kimura, K. *et al.* (1996). Regulation of myosin phosphatase by Rho and Rho-associated kinase (Rho- kinase) [see comments]. Science *273*, 245–248.

Kimura, K., Tsuji, T., Takada, Y., Miki, T., and Narumiya, S. (2000). Accumulation of GTP-bound RhoA during cytokinesis and a critical role of ECT2 in this accumulation. J. Biol. Chem. *275*, 17233–17236.

Kosako, H. *et al.* (1999). Specific accumulation of Rho-associated kinase at the cleavage furrow during cytokinesis: cleavage furrow-specific phosphorylation of intermediate filaments. Oncogene *18*, 2783–2788.

Kosako, H., Yoshida, T., Matsumura, F., Ishizaki, T., Narumiya, S., and Inagaki, M. (2000). Rho-kinase/ROCK is involved in cytokinesis through the phosphorylation of myosin light chain and not ezrin/radixin/moesin proteins at the cleavage furrow. Oncogene *19*, 6059–6064.

Laemmli, U.K. (1970). Cleavage of structural proteins during the assembly of the head of bacteriophage T4. Nature *227*, 680–685.

Leung, T., Chen, X.Q., Manser, E., and Lim, L. (1996). The p160 RhoA-binding kinase ROK alpha is a member of a kinase family and is involved in the reorganization of the cytoskeleton. Mol. Cell. Biol. *16*, 5313–5327.

Madaule, P., Eda, M., Watanabe, N., Fujisawa, K., Matsuoka, T., Bito, H., Ishizaki, T., and Narumiya, S. (1998). Role of citron kinase as a target of the small GTPase Rho in cytokinesis. Nature *394*, 491–494.

Madaule, P., Furuyashiki, T., Eda, M., Bito, H., Ishizaki, T., and Narumiya, S. (2000). Citron, a Rho target that affects contractility during cytokinesis. Microsc. Res. Tech. *49*, 123–126.

Matsumura, F., Ono, S., Yamakita, Y., Totsukawa, G., and Yamashiro, S. (1998). Specific localization of serine 19 phosphorylated myosin II during cell locomotion and mitosis of cultured cells. J. Cell Biol. *140*, 119–129.

Murata-Hori, M., Fukuta, Y., Ueda, K., Iwasaki, T., and Hosoya, H. (2001). HeLa ZIP kinase induces diphosphorylation of myosin II regulatory light chain, and reorganization of actin filaments in nonmuscle cells. Oncogene. *20*, 8175–8183.

Murata-Hori, M., Suizu, F., Iwasaki, T., Kikuchi, A., and Hosoya, H. (1999). ZIP kinase identified as a novel myosin regulatory light chain kinase in HeLa cells. FEBS Lett. *451*, 81–84.

Nakano, K., Takaishi, K., Kodama, A., Mammoto, A., Shiozaki, H., Monden, M., and Takai, Y. (1999). Distinct actions and cooperative roles of ROCK and mDia in Rho small G protein-induced reorganization of the actin cytoskeleton in Madin-Darby canine kidney cells. Mol. Biol. Cell *10*, 2481–2491.

Perrie, W.T., and Perry, S.V. (1970). An electrophoretic study of the low-molecular-weight components of myosin. Biochem. J. *119*, 31–38.

Poperechnaya, A., Varlamova, O., Lin, P.J., Stull, J.T., and Bresnick, A.R. (2000). Localization and activity of myosin light chain kinase isoforms during the cell cycle. J. Cell Biol. *151*, 697–708.

Ridley, A.J. (2001). Rho family proteins: coordinating cell responses. Trends Cell Biol. *11*, 471–477.

Sakurada, K., Ikuhara, T., Seto, M., and Sasaki, Y. (1994). An antibody for phosphorylated myosin light chain of smooth muscle: application to a biochemical study. J. Biochem. (Tokyo) *115*, 18–21.

Sakurada, K., Seto, M., and Sasaki, Y. (1998). Dynamics of myosin light chain phosphorylation at Ser19 and Thr19/Ser19 in smooth muscle cells in culture. Am. J. Physiol. (Cell Physiol. 43) *274*, c1563–c1572.

Sellers, J.R. (1991). Regulation of cytoplasmic and smooth muscle myosin. Curr. Opin. Cell Biol. *3*, 98–104.

Settleman, J. (2001). Rac 'n Rho: the music that shapes a developing embryo. Dev. Cell *1*, 321–331.

Somlyo, A.P., and Somlyo, A.V. (2000). Signal transduction by G-proteins, rho-kinase and protein phosphatase to smooth muscle and non-muscle myosin II. J. Physiol. *522* (Pt 2), 177–185.

Totsukawa, G., Yamakita, Y., Yamashiro, S., Hartshorne, D.J., Sasaki, Y., and Matsumura, F. (2000). Distinct roles of ROCK (Rho-kinase) and MLCK in spatial regulation of MLC phosphorylation for assembly of stress fibers and focal adhesions in 3T3 fibroblasts. J. Cell Biol. *150*, 797–806.

Umemoto, S., Bengur, A.R., and Sellers, J.R. (1989). Effect of multiple phosphorylations of smooth muscle and cytoplasmic myosins on movement in an in vitro motility assay. J. Biol. Chem. *264*, 1431–1436.

Watanabe, N., Kato, T., Fujita, A., Ishizaki, T., and Narumiya, S. (1999). Cooperation between mDia1 and ROCK in Rho-induced actin reorganization. Nat. Cell Biol. *1*, 136–143.

Yamakita, Y., Yamashiro, S., and Matsumura, F. (1994). In vivo phosphorylation of regulatory light chain of myosin II during mitosis of cultured cells. J. Cell Biol. *124*, 129–137.

Yamashiro, S., Yamakita, Y., Ono, S., and Matsumura, F. (1998). Fascin, an actin-bundling protein, induces membrane protrusions and increases cell motility of epithelial cells. Mol. Biol. Cell *9*, 993–1006.

Zeng, Q., Lagunoff, D., Masaracchia, R., Goeckeler, Z., Cote, G., and Wysolmerski, R. (2000). Endothelial cell retraction is induced by PAK2 monophosphorylation of myosin II. J. Cell Sci. *113*(Pt 3), 471–482.

Zhang, W., Vazquez, L., Apperson, M., and Kennedy, M.B. (1999). Citron binds to PSD-95 at glutamatergic synapses on inhibitory neurons in the hippocampus. J. Neurosci. *19*, 96–108.

MOLECULAR AND CELLULAR BIOLOGY, July 2003, p. 5043–5055 Vol. 23, No. 14
0270-7306/03/$08.00+0 DOI: 10.1128/MCB.23.14.5043–5055.2003

Targeted Disruption of the Mouse Rho-Associated Kinase 2 Gene Results in Intrauterine Growth Retardation and Fetal Death

Dean Thumkeo, Jeongsin Keel,† Toshimasa Ishizaki, Masaya Hirose,‡ Kimiko Nonomura, Hiroko Oshima, Masanobu Oshima, Makoto M. Taketo, and Shuh Narumiya*

Department of Pharmacology, Kyoto University Faculty of Medicine, Sakyo-ku, Kyoto 606-8501, Japan

Received 12 December 2002/Returned for modification 31 January 2003/Accepted 28 April 2003

Rho-associated kinase (ROCK), including the ROCK-I and ROCK-II isoforms, is a protein kinase involved in signaling from Rho to actin cytoskeleton. However, in vivo functions of each ROCK isoform remain largely unknown. We generated mice deficient in ROCK-II by gene targeting. ROCK-II$^{-/-}$ embryos were found at the expected Mendelian frequency until 13.5 days postcoitum, but approximately 90% died thereafter in utero. ROCK-II$^{-/-}$ mice of both genders that survived were born runts, subsequently developed without gross abnormality, and were fertile. Whole-mount staining for a knocked-in *lacZ* reporter gene revealed that ROCK-II was highly expressed in the labyrinth layer of the placenta. Disruption of architecture and extensive thrombus formation were found in the labyrinth layer of ROCK-II$^{-/-}$ mice. While no obvious alteration in actin filament structures was found in the labyrinth layer of ROCK-II$^{-/-}$ placenta and stress fibers were formed in cultured ROCK-II$^{-/-}$ trophoblasts, elevated expression of plasminogen activator inhibitor 1 was found in ROCK-II$^{-/-}$ placenta. These results suggest that ROCK-II is essential in inhibiting blood coagulation and maintaining blood flow in the endothelium-free labyrinth layer and that loss of ROCK-II leads to thrombus formation, placental dysfunction, intrauterine growth retardation, and fetal death.

The small GTPase Rho, including RhoA, -B, and -C, works as a molecular switch and regulates various cellular processes, such as cell adhesion, migration, cytokinesis, proliferation, and transformation (3, 28). The Rho-regulated adhesion of cell to substrate is typically seen as induction of focal adhesions and stress fibers in fibroblasts. These Rho actions are exerted by combined actions of downstream Rho effectors. A variety of Rho effectors have been identified. Of the Rho effectors, Rho-associated kinase (ROCK; also known as ROK or Rho kinase) (12, 17, 19, 22) has been studied most extensively and has been suggested to be one of the major Rho effectors mediating Rho signal to reorganize the actin cytoskeleton. Indeed, it is known that ROCK regulates several steps of actin dynamics. ROCK phosphorylates the regulatory subunit of myosin light-chain phosphatase and inhibits its activity, thereby increasing the level of phosphorylated myosin light chain and inducing actomyosin-based contraction seen in smooth muscle contraction and neurite retraction (7). ROCK also phosphorylates and activates LIM kinase. Activated LIM kinase in turn phosphorylates an actin-binding protein, coffilin/actin-depolymerizing factor (ADF), and inactivates its actin depolymerizing and severing activity, which leads to inhibition of actin filament disassembly (18). These ROCK actions on actin dynamics combined together contribute to Rho-induced actomyosin organization seen in stress fiber formation.

We previously introduced a synthetic compound, Y-27632, as a specific ROCK inhibitor (34). Since our report, this compound has been used extensively to examine not only the actions of ROCK in cultured cells but also its roles in vivo in the body. While these studies have provided significant insights into the role of ROCK in several pathological processes, such as hypertension and tumor invasion (14, 34), the involvement and significance of the ROCK-mediated pathway in development and homeostasis of the body are unknown, because Y-27632 is a relatively short-acting drug. There are also several Y-27632-sensitive and supposedly ROCK-mediated processes, such as regulation of specific genes, which appear not to be mediated through ROCK actions on actin dynamics and have to be confirmed and assessed by means other than the use of Y-27632 (36). Furthermore, because ROCK consists of two isoforms, ROCK-I and -II (12, 17, 19, 22) and Y-27632 suppresses the activity of both isoforms, the specific function of an individual isoform could not be elucidated by the use of this compound.

The mammalian placenta is the organ in which respiratory gases, nutrients, and wastes are exchanged between the maternal and fetal circulation systems. This transplacental exchange provides all the metabolic demands for fetal growth and development. Because the rate of this exchange depends primarily on blood flow, decreased blood flow in the maternal or fetal side can induce intrauterine growth retardation (IUGR) of the embryo (26). The site of the transplacental exchange is the labyrinth layer of the placenta, in which the maternal blood flow is countercurrent to the fetal capillary flow through the trophoblast cell layer. The maternal blood flows into the base of the labyrinth through a few straight canals, perfuses a dense network of sinusoids, and percolates back to the maternal side through a number of smaller canals (2). A unique feature of this maternal circulation is that, distinct from blood vessels throughout the body, the passage is not lined by endothelial cells but by specialized trophoblasts. How the homeostasis of

* Corresponding author. Mailing address: Department of Pharmacology, Kyoto University Faculty of Medicine, Kyoto 606-8501, Japan. Phone: 81-75-753-4392. Fax: 81-75-753-4693. E-mail: snaru@mfour.med.kyoto-u.ac.jp.

† Died on 6 September 2000.

‡ Present address: Department of Gynecology, Shiga University of Medical Science, Ohtsu 520-2192, Japan.

this maternal blood circulation is maintained without endothelium is poorly understood.

To explore the specific function of mouse ROCK-II (mROCK-II), we generated ROCK-II-deficient mice by knocking in a *lacZ* reporter gene. Most ROCK-II-deficient mice die in utero with unusually large thrombi in the labyrinth layer of the placenta, and the survivors were born runts. This phenotype is strongly reminiscent of human IUGR. Using a whole-mount staining technique for the mROCK-II–*lacZ* reporter gene, we observed that ROCK-II is strongly expressed in the labyrinth layer of the placenta. Interestingly, while we found strong F-actin architecture in the labyrinth layer, there was no significant difference in the F-actin structure in the tissues of wild-type and ROCK-II$^{-/-}$ mice. Analysis of gene expression in the placenta revealed elevated expression of plasminogen activator inhibitor 1 (PAI-1) in ROCK-II$^{-/-}$ placenta, suggesting decreased fibrinolytic activity (4) that might be the primary cause of large thrombus formation in the labyrinth layer, placental dysfunction, IUGR, and fetal death of ROCK-II$^{-/-}$ mice.

MATERIALS AND METHODS

Generation of the targeting vector. The multicloning site of pBluescript SK+ (Stratagene) was modified to contain restriction enzyme sites as follows: *Sac*I-*Sac*II-*Not*I-*Xba*I-*Kpn*I-*Eco*RV-*Bam*HI-*Sal*I-*Pst*I-*Nhe*I-*Asc*I-*Aat*II-*Cla*I-*Sal*I-*Nco*I-*Asc*I (pBSKV4). A 129/SvJ lambda FIXII genomic library (Stratagene) was used, and several clones containing various parts of the mROCK-II gene were isolated. The targeting vector was constructed as follows. A 2.4-kb fragment containing 34 bp of the third exon (defined in the National Center for Biotechnology Information mouse genome sequencing database), encoding part of the kinase domain and its 5′ flanking region, was generated by PCR amplification with 5′-GGG GGA TAT CTA CTC ACA TCT GAA GAT TTG G-3′ as a forward primer and 5′-GGG GAT CGA TCT GTA AAC CTC TGA TTT TTT TCA-3′ as a reverse primer. The fragment was digested with *Eco*RV and *Cla*I and subcloned into pBSKV4. The plasmid DNA was then cut open with *Kpn*I and *Eco*RV, and a 0.5-kb *Kpn*I/*Eco*RV 5′ fragment obtained from partial digestion of mROCK-II DNA was introduced. The resulting vector was digested with *Kpn*I, and a 7-kb *Kpn*I fragment of mROCK-II DNA was then introduced to generate a long arm (9.9 kb) that extends from a 5′ *Kpn*I site to 34 bp 3′ downstream to the splicing acceptor of exon 3 of mROCK-II (Fig. 1A). This long arm was then fused with the *Cla*I/*Sal*I fragment containing the β-galactosidase gene. The resulting plasmid was opened by digestion with *Sal*I and *Nco*I, and the *Sal*I/*Nco*I fragment containing the phosphoglycerate kinase (PGK)-thymidine kinase (TK) cassette was inserted. A 1.1-kb short arm corresponding to the 3′ sequence downstream of exon 3 was amplified by PCR with 5′-CCC CGG ATC CAT CAT AGC AGC TGA ATA GTT C-3′ as a forward primer and 5′-CCC CCC CGG GCA ACC CAT AGG GAG TAC TC-3′ as a reverse primer and inserted into a PGK-*Neo* cassette, which was then digested with *Xho*I and *Sma*I. The fragment was then inserted into the above vector to generate the final targeting construct.

Genotyping. Genotyping was performed by Southern blot analysis or PCR, using genomic DNA prepared from embryonic stem (ES) cells, embryonic visceral yolk sacs, or the tails of mice (Fig. 1A). PCR primers were 5′-CAG AGG TTT ACA GAT GAA AGC GGA AG-3′ (a forward primer for wild-type allele), 5′-GCT CCA GAC TGC CTT GGG AAA AGC-3′ (a forward primer for the targeted allele), and 5′-CTG TAA TCC AGC ACC TGT GAA GTG G-3′ (a reverse primer for the wild-type and targeted alleles).

Generation of ROCK-II-deficient mice. The targeting vector linearized with *Not*I was electroporated into ES cells, line RW4 (Genome System). Two hundred G418-resistant clones were screened, and homologous recombination was verified in two clones by PCR genotyping. Cells of the positive clones were injected into blastocysts, and the chimeric offspring obtained were mated to C57BL/6J females. ROCK-II$^{+/-}$ heterozygous mice were then intercrossed to produce homozygous mutants (ROCK-II$^{-/-}$). Mice were treated according to the guidelines for protection of experimental animals of Kyoto University, and all experimental procedures were approved by the Committee on Animal Research of the Kyoto University Faculty of Medicine.

Western blot analysis. Whole embryos 13.5 days postcoitum (dpc) or whole brains of adult mice were lysed in lysis buffer containing 50 mM Tris-HCl (pH 7.5), 150 mM NaCl, 1% Nonidet P-40 (NP-40), 0.5% deoxycholate, and protease inhibitors (Complete tablet; Roche Diagnostics). After the protein concentrations were determined, one-third volume of 4× Laemmli buffer was added to the mixture, which was then boiled for 5 min. The lysates were subjected to sodium dodecyl sulfate (SDS)-polyacrylamide gel electrophoresis under reducing conditions. Separated proteins were transferred to nitrocellulose membranes and probed with rabbit anti-ROCK-II antibody raised against amino acids 775 to 860 of human ROCK-II (H-85; Santa Cruz Biotechnology), rabbit anti-ROCK-I antiserum (12), or mouse anti-β-tubulin antibody (Sigma).

Whole-mount β-galactosidase staining. ROCK-II$^{-/-}$, ROCK-II$^{+/-}$, and wild-type embryos and placentas were isolated at 13.5 dpc. The samples were fixed for 30 min at 4°C with 2% paraformaldehyde in phosphate-buffered saline (PBS) containing 2 mM $MgCl_2$, 5 mM EGTA (pH 8.0), and 0.02% NP-40. The samples were washed and stained for 16 h at 30°C for β-galactosidase in 5-bromo-4-chloro-3-indolyl-β-D-galactopyranoside (X-Gal) solution [1-mg/ml X-Gal solution containing 5 mM $K_3Fe(CN)_6$, 5 mM $K_4Fe(CN)_6$, 2 mM $MgCl_2$, 0.01% SDS, and 0.02% NP-40].

Histology. Three adult ROCK-II$^{-/-}$ mice, one male and two females, were sacrificed, and various organs were isolated. For paraffin sections, the isolated organs, embryo, and placenta were fixed in 4% paraformaldehyde. They were then embedded in paraffin and cut into 7-μm-thick sections. Hematoxylin and eosin staining was performed using a standard protocol. Immunohistochemistry with anti-platelet-endothelial cell adhesion molecule (PECAM) antibody (MEC13.3; Pharmingen) was performed on the paraffin-wax sections as previously described (11). To stain F-actin in tissue, placentas were fixed in 2% paraformaldehyde at 4°C for 2 h and immersed in 20% sucrose for 2 h and then in PBS containing 25% sucrose overnight at 4°C. The placentas were then frozen in Tissue-Tek OCT compound in liquid nitrogen and were cut into serial 10-μm-thick sections using a cryostat. The sections were incubated with Texas red phalloidin (Molecular Probes) for 10 min at room temperature. After the sections were washed with PBS, they were examined with a Zeiss LSM 510 confocal imaging system.

Primary culture of trophoblasts from the labyrinth layer. Cells were prepared from the labyrinth layer of the placenta at 13.5 dpc as described previously (31) with modifications. Briefly, embryos with their encapsulating decidual tissue were removed from the uterus and washed with PBS. The placenta was dissected free from decidual tissue and yolk sac and umbilical vessels, and the labyrinth layer was isolated and cut into small pieces. The tissue pieces were then treated with 0.025% trypsin and 0.5 mg of DNase I per ml in PBS for 10 min at 37°C. The pieces were gently triturated 10 times using a Pasteur pipette. Digestion was terminated by adding Dulbecco modified Eagle medium (DMEM) containing 10% heat-inactivated fetal calf serum (FCS). The mixture was then filtered and centrifuged at 100 × *g* for 10 min at room temperature. Cells were suspended in DMEM containing 10% FCS and plated onto a noncoated or fibronectin-coated cover glass in 35-mm-diameter dishes. After 24 h of culture, cells were washed once with PBS and fixed with 3.7% paraformaldehyde for 15 min at room temperature. The cells were then permeabilized with PBS containing 0.1% Triton X-100 for 5 min and stained for F-actin with Texas red phalloidin (Molecular Probes). Optical images were obtained with a confocal imaging system (Bio-Rad Laboratories MRC1024 or Zeiss LSM510 confocal imaging system).

DNA microarray analysis. The placenta was excised from ROCK-II$^{+/-}$ and ROCK-II$^{-/-}$ dpc 13.5 embryos of the same litter. Total RNA was prepared by using RNeasy kit (Qiagen). Affymetrix GeneChip expression analysis using a MG-U74Av2 chip (Affymetrix Inc., Santa Clara, Calif.) was performed according to the manufacturer's protocol. Data were analyzed with the Affymetrix GeneChip Expression Analysis software (version 4.0).

RT-PCR analysis. Total RNA (10 ng) prepared from placentas of ROCK-II$^{+/-}$ and ROCK-II$^{-/-}$ dpc 13.5 embryos was used as templates. Reverse transcription-PCR (RT-PCR) was performed by using the Superscript One-Step RT-PCR system (Invitrogen). The primers used to detect PAI-1 expression were 5′-ATG AGA TCA GTA CTG CGG ATG CCA TCT TTG-3′ (sense primer) and 5′-GCA CAG AGA CGG TGC TGC CAT CAG ACT TGT-3′ (antisense primer). Glyceraldehyde-3-phosphate dehydrogenase (GAPDH), a housekeeping gene, was used as a control. Reaction conditions were optimized to obtain amplification within the logarithmic phase of the reaction reproducibly.

Northern blot analysis. For Northern blot analysis, total RNA from the placentas of ROCK-II$^{+/-}$ and ROCK-II$^{-/-}$ dpc 13.5 embryos was prepared by using a RNeasy kit (Qiagen). RNA (10 μg) was separated on a 0.7% agarose gel containing 2.1% formaldehyde and transferred to a Hybond-N+ membrane (Amersham Pharmacia Biotech). A 900-bp *Nco*I/*Hin*dIII fragment of the mouse PAI-1 cDNA (24) was used as a probe. GAPDH was used as a control. The probe was labeled with [α-^{32}P]dCTP using Ready-To-Go (Amersham Pharmacia), and hybridization was done in ULTRAhyb (Ambion). The filter was washed twice for 5 min in 2× SSC–0.1% SDS (1× SSC is 0.15 M NaCl plus 0.015 M sodium

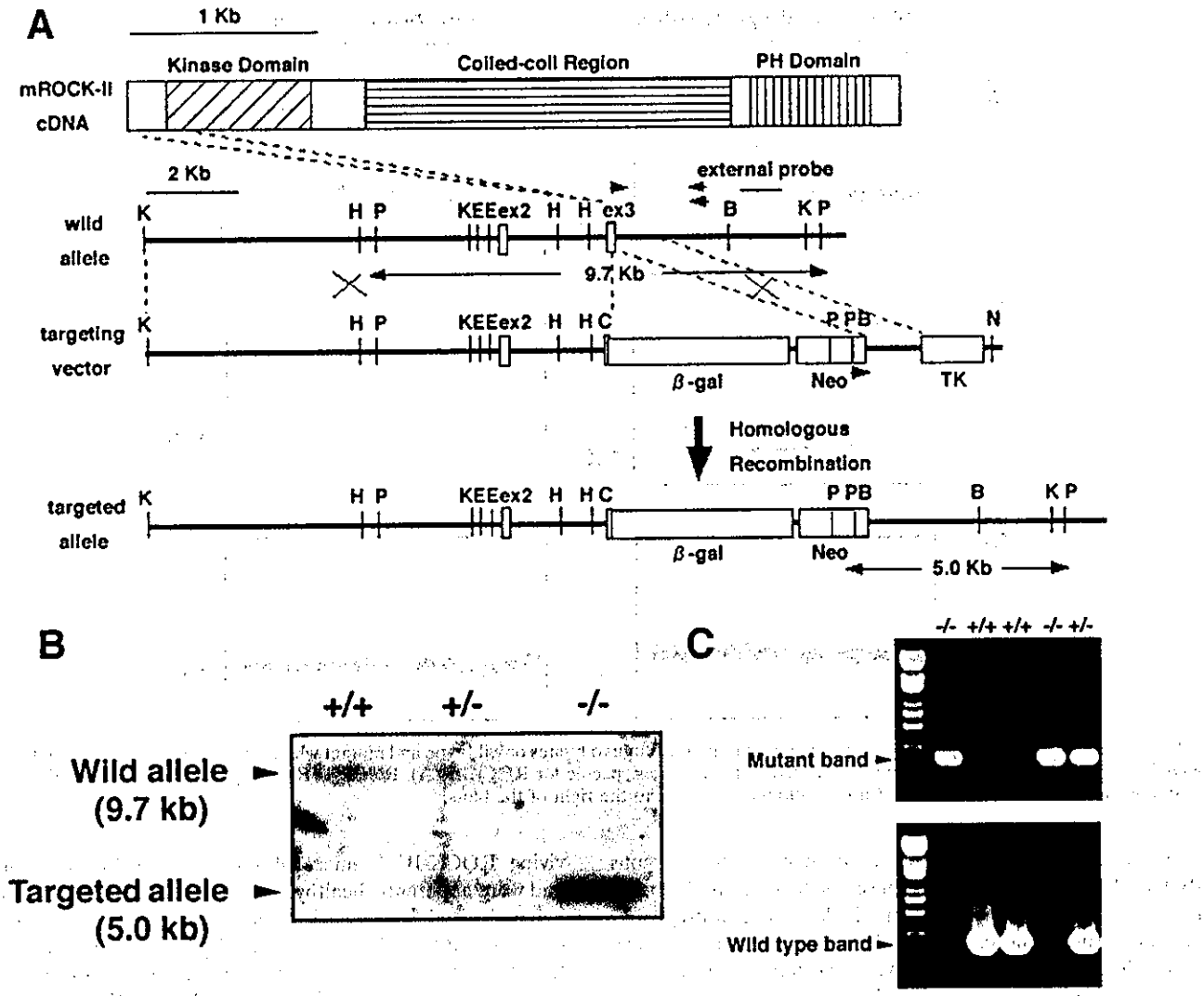

FIG. 1. Generation of ROCK-II-deficient mice. (A) Targeting strategy. Schematic representations of the domain structure of ROCK-II, the wild-type ROCK-II allele, targeting vector, and the targeted allele are shown. The positions of β-galactosidase (β-gal), neomycin resistance (Neo), and thymidine kinase (TK) genes, restriction sites *Kpn*I (K), *Hin*dIII (H), *Pst*I (P), *Eco*RV (E), *Bam*HI (B), *Cla*I (C), and *Not*I (N), and exons 2 (ex2) and 3 (ex3) are shown. The positions of primers for PCR analysis are indicated by the arrowheads. The external probe is a unique 3′ genomic probe that distinguishes the wild-type 9.7-kb *Pst*I fragment from a 5-kb *Pst*I fragment generated by the targeted alleles. (B) Southern blot analysis of genomic DNA obtained from visceral yolk sacs at 13.5 dpc. (C) Genotyping by PCR on genomic DNA obtained from visceral yolk sacs at 13.5 dpc.

citrate) at 42°C and twice for 15 min in 0.1× SSC–0.1% SDS at 42°C and subjected to film autoradiography.

RESULTS

Generation and embryonic lethality of mROCK-II-deficient mice. We disrupted the mROCK-II gene by replacing most of exon 3, which encodes part of the kinase domain, with genes for β-galactosidase and neomycin resistance (Fig. 1A). Mice with the chimeric mutant allele were generated and mated with C57BL/6 females to produce heterozygous ROCK-II$^{+/-}$ mice, which were then intercrossed. The genotypes of the offspring were identified by Southern blot analysis and PCR on DNA obtained from the visceral yolk sacs or tails of mice (Fig. 1B and C). Disruption of the mROCK-II gene was also confirmed by Western blot analysis for ROCK-II protein. A 160-kDa band of ROCK-II protein was detected in wild-type dpc 13.5 embryo lysates and in whole-brain lysates of adult mice (Fig. 2A). The amount of ROCK-II protein in ROCK-II$^{+/-}$ embryo lysates decreased to half the amount in wild-type dpc 13.5 embryo lysates, and ROCK-II protein was absent in ROCK-II$^{-/-}$ embryos (Fig. 2A). On the other hand, there was no difference in the level of ROCK-I protein in the embryonic lysates or whole-brain lysates (Fig. 2B), indicating that the amount of ROCK-I did not increase to compensate for the loss of ROCK-II.

Analysis of the genotype distribution in offspring from heterozygous mating by chi-square (χ^2) analysis revealed that the homozygous ROCK-II$^{-/-}$ mice at dpc 18.5 are significantly underrepresented ($P < 0.05$) from the value predicted by Mendelian inheritance. We found that only 7.7% of embryos at dpc

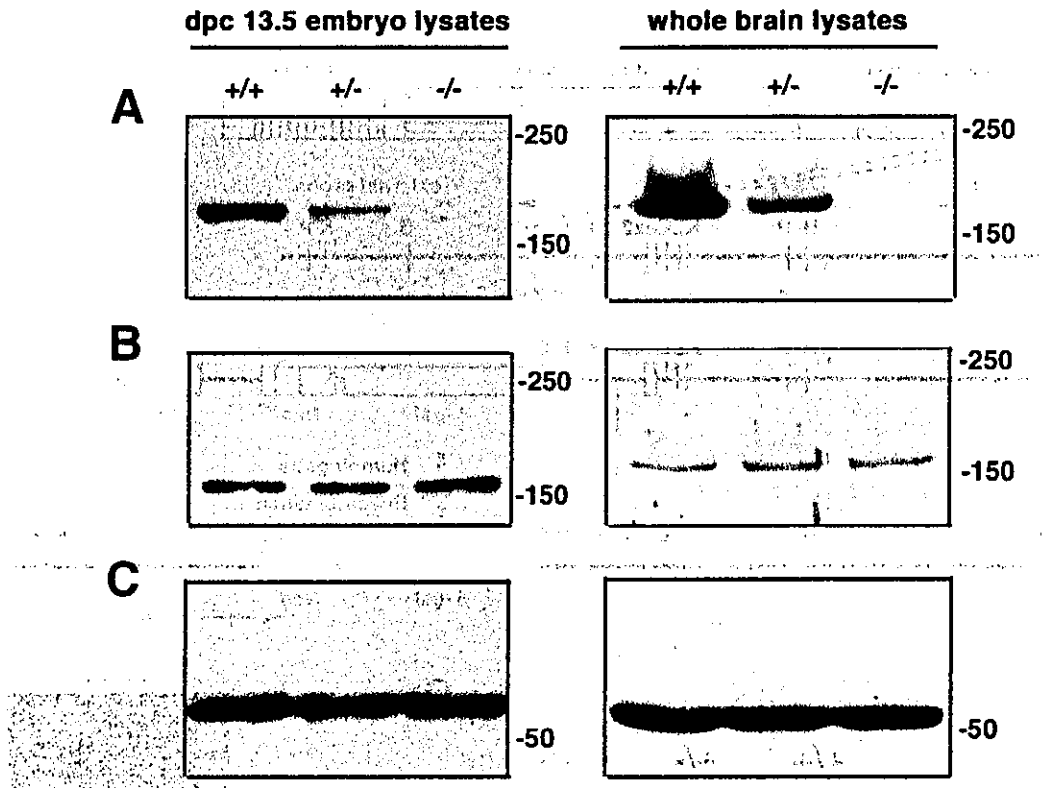

FIG. 2. Western blot analysis. Wild-type and mutant dpc 13.5 embryo lysates or wild-type and mutant whole adult brain lysates of ROCK-II$^{+/+}$, ROCK-II$^{+/-}$, and ROCK-II$^{-/-}$ mice were probed with antibodies specific for ROCK-II (A), ROCK-I (B), and β-tubulin (C), respectively. The positions of molecular mass markers (in kilodaltons) are shown to the right of the blots.

18.5 and only 5.3% of the animals born had a homozygous ROCK-II genotype (Table 1). These results indicate that most ROCK-II$^{-/-}$ embryos died during the late stage of pregnancy in utero. Furthermore, it is unlikely that there is a critical period for the embryo morbidity, as the number of homozygous embryos gradually decreased.

Growth retardation was observed in the embryos that survived the late stage of pregnancy (Fig. 3A), and the ROCK-II$^{-/-}$ mice that survived were always runts. Most of the surviving ROCK-II$^{-/-}$ mice subsequently developed normally and were apparently healthy. One mouse lived 11 months, and two males and two females tested were fertile (Table 1). However, two ROCK-II$^{-/-}$ mice that displayed severe growth retardation (were about 40 to 50% the size of the control mice) died after 3 to 4 weeks. Three adult mROCK-II$^{-/-}$ mice were sacrificed and examined for gross and histological abnormalities. Examination of tissue sections stained with hematoxylin and eosin revealed no obvious abnormalities in the brain and

TABLE 1. Genotypes of offspring obtained by crossing of ROCK-II mutant mice[a]

Cross and stage	Total no. of offspring	No. of mice with genotype:			No. resorbed	χ^2 value	*P* value (df = 2)
		+/+	+/−	−/−			
♂(+/−) × ♀ (+/−)							
10.5 dpc	50	10	27	13	0	3.35	0.19
12.5 dpc	21	6	11	4	0	0.75	0.69
13.5 dpc	110	23	45	22 (1)[b]	10	0.07	0.97
15.5 dpc	73	18	35	10 (2)	10	3.58	0.16
18.5 dpc	51	13	25 (2)	4 (1)	9	6.27	0.04
Adult	122	38	76	8 (2)	NA[c]	23.68	0.00
♂ (−/−) × ♀ (+/−)							
Adult	24	0	23	1	NA	9.59	0.01
♂ (+/−) × ♀ (−/−)							
Adult	12	0	12	0	NA	6.00	0.05

[a] The genotypes of the wild-type (ROCK-II$^{+/+}$), ROCK-II$^{+/-}$, and ROCK-II$^{-/-}$ mice are shown as +/+, +/−, and −/−, respectively.
[b] The number of dead animals is shown in parentheses.
[c] NA, not applicable.

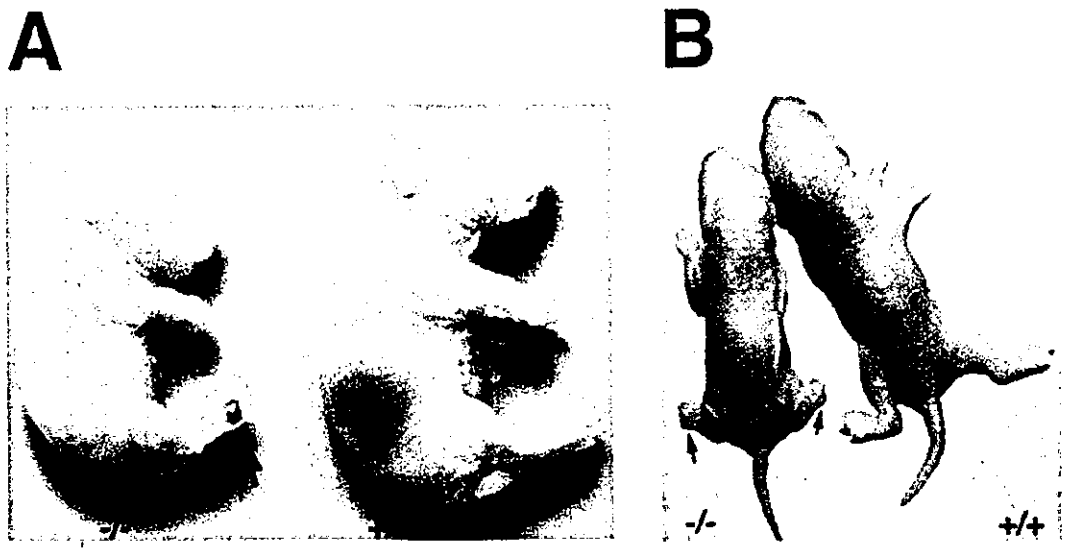

FIG. 3. Growth retardation of ROCK-II$^{-/-}$ mice. Wild-type (ROCK-II$^{+/+}$) and ROCK-II$^{-/-}$ dpc 18.5 embryos (A) and neonates (B) are shown. Note that the ROCK-II$^{-/-}$ mouse was a runt. Hematomas in the hind limbs of the ROCK-II$^{-/-}$ mouse are indicated by arrows.

spinal cord, the heart and aorta, the lung and trachea, the kidney and bladder, endocrine organs (such as the thyroid, pituitary, and adrenal glands), hematopoietic and lymphoid organs (such as the bone marrow, spleen, thymus, and mesenteric lymph nodes), the gastrointestinal tract from the tongue to the rectum, the reproductive organs (such as testis, epididymis, seminal vesicle, prostate gland, ovary, and uterus), and the epidermis and dermis of the skin (data not shown).

High expression of mROCK-II in the labyrinth layer of the placenta and disruption of its architecture in mROCK-II$^{-/-}$ mice. Because a *lacZ* reporter gene was knocked in frame with the initiator methionine of mROCK-II in the targeting construct, we examined the pattern of expression of the mROCK-II gene by whole-mount β-galactosidase staining. As shown in a 13.5 dpc ROCK-II$^{+/-}$ embryo, X-Gal staining was observed in many locations throughout the embryo, including the heart, dorsal root ganglions, and umbilical blood vessels (Fig. 4A). Spotted staining was also observed in the liver of the embryo. In the placenta, strong X-Gal staining was observed in the labyrinth layer (Fig. 4B and C). Detailed inspection revealed that trophoblasts in the labyrinth layer were uniformly stained (Fig. 4D). In addition, a blood vessel in the chorionic plate, apparently the umbilical artery, was positively stained (Fig. 4E). In all tissues examined thus far, the patterns of X-Gal staining of ROCK-II$^{+/-}$ and ROCK-II$^{-/-}$ mice were identical or highly similar (data not shown).

The above findings that most ROCK-II$^{-/-}$ mice die in utero and the homozygotes that survived were born runts but subsequently caught up in growth indicated a defect(s) in the interaction of the embryo and placenta in ROCK-II$^{-/-}$ mice. To clarify this issue, a litter of placentas and embryos were isolated at 10.5 to 14.5 dpc from the uterus of a heterozygous mother mated with a heterozygous male and examined. No significant abnormality was observed in eight ROCK-II$^{-/-}$ placentas prior to 11.5 dpc (data not shown). However, as shown in Fig. 5A and B, a number of large blood clots were typically visible in the placentas of ROCK-II$^{-/-}$ mice from 12.5 dpc on, but not in those of wild-type littermates. Approximately 80% of ROCK-II$^{-/-}$ placentas showed this abnormality to various extents. Histological examination of the placentas of ROCK-II$^{-/-}$ mice at 12.5 and 13.5 dpc revealed that multiple large thrombi were present in the labyrinth layer, increased in size and number with time, and disrupted its normal architecture (Fig. 5C to F). In some cases, approximately 10% of the total volume of the labyrinth layer was occupied by thrombi. Small thrombi occasionally formed in the placentas of wild-type and heterozygous littermates (Fig. 5C and data not shown) and grew. However, the prevalence and size of thrombi in the ROCK-II$^{-/-}$ placenta were unusual. It is evident that these thrombi were formed in the labyrinth layer of the maternal circulation system, because they contained enucleated erythrocytes and were not in the fetal circulation system lined by the endothelium (Fig. 5G).

No overt abnormalities in actin fiber structure in the labyrinth layer and in labyrinth layer-derived cultured trophoblasts of ROCK-II$^{-/-}$ mice. The above results suggested that loss of ROCK-II induced the thrombogenic tendency locally in the labyrinth layer of ROCK-II$^{-/-}$ mice. Because ROCK mediates a Rho signal to organize the actin cytoskeleton involved in cell-substrate adhesion and ROCK-II is abundantly expressed in trophoblasts in the labyrinth layer (Fig. 4B), we first suspected that loss of ROCK-II might affect the cytoarchitecture of trophoblasts and tear them off under the stress of the shearing force. To examine this issue, we first compared the architecture of actin in the labyrinth layer in wild-type and ROCK-II$^{-/-}$ mice. We also cultured trophoblasts from the labyrinth layers of wild-type and ROCK-II$^{-/-}$ mice and compared their actin cytoskeleton.

For an accurate comparison, we placed tissue sections from mice with the two genotypes on the same glass slide and performed staining and microscopic observation of the two simultaneously. We also stained and examined the cell cultures from the two genotypes side by side. As shown in Fig. 6A, a strong and complex network of actin fibers was found throughout the

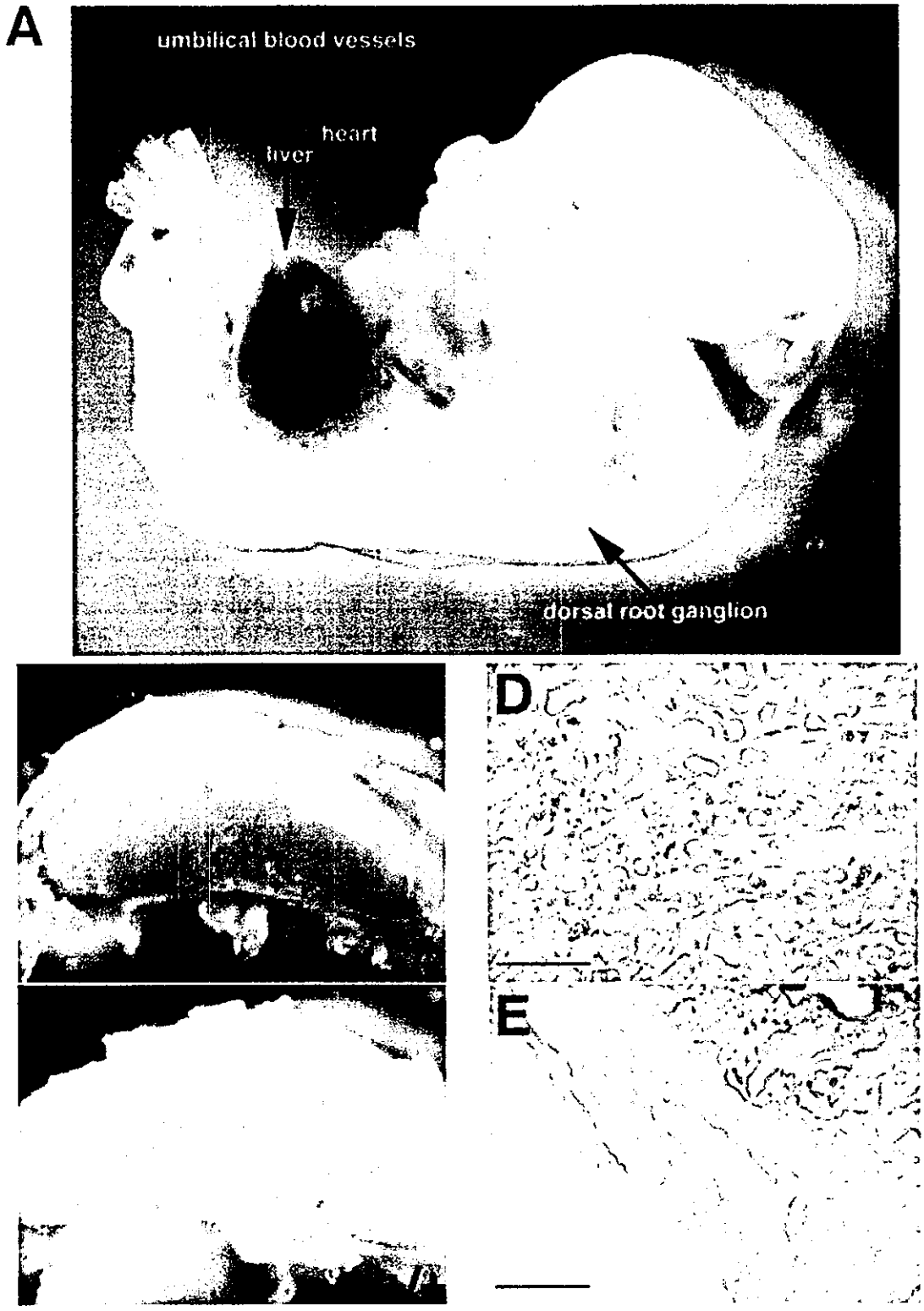

FIG. 4. ROCK-II expression in 13.5-dpc embryo and placenta as revealed by X-Gal staining of the *lacZ* reporter gene. (A) Expression in the embryo at 13.5 dpc. X-Gal staining is detected in umbilical blood vessels, heart, and dorsal root ganglion. (B and C) Expression in the placenta. Strong X-Gal staining is found in the labyrinth layer of ROCK-II$^{-/-}$ placenta (B), which is rich in vasculature as shown in ROCK-II$^{+/+}$ placenta (C). (D) Uniform X-Gal staining in trophoblasts in the labyrinth layer. (E) Expression of the ROCK-II-*lacZ* reporter gene in a blood vessel in the chorionic plate. Parallel staining for actin (data not shown) indicates that the vessel stained with X-Gal (below) is the umbilical artery, while the vessel devoid of the X-Gal staining (above) is a vein. Bars, 100 μm.

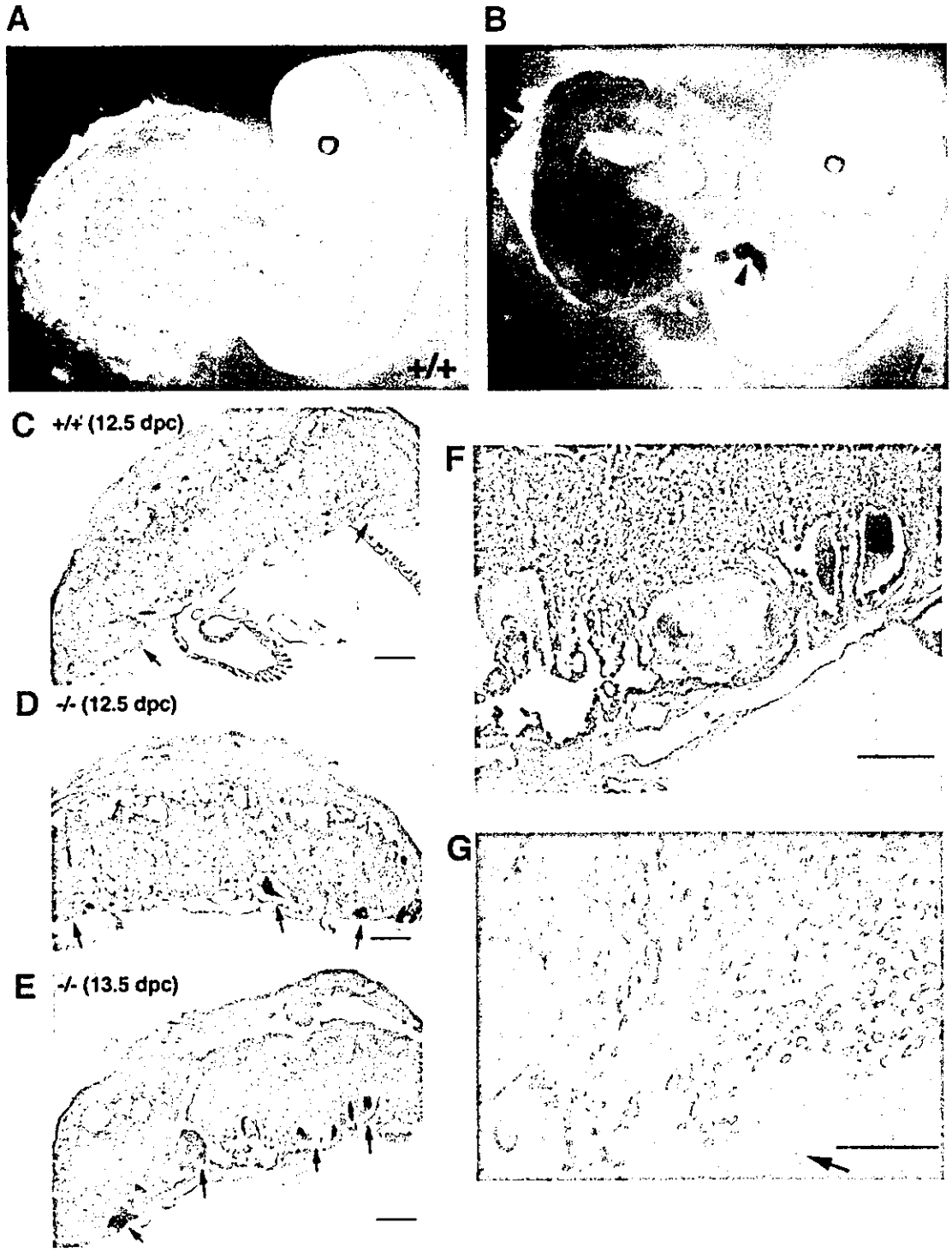

FIG. 5. Morphology and histology of wild-type (ROCK-II$^{+/+}$) and ROCK-II$^{-/-}$ embryos and placentas. (A and B) Embryos isolated together with their placentas. Blood clots found in the ROCK-II$^{-/-}$ placenta (arrows) and hemorrhage in the hind limb of the ROCK-II$^{-/-}$ embryo (arrowhead) are indicated. (C to F) Hematoxylin and eosin staining of a 12.5-dpc wild-type placenta (C), a 12.5-dpc ROCK-II$^{-/-}$ placenta (D), and a 13.5-dpc ROCK-II$^{-/-}$ placenta (E). Panel F shows a higher-magnification view of the labyrinth layer shown in panel E. (G) Immunohistochemical staining of the labyrinth layer of a ROCK-II$^{-/-}$ placenta with an anti-PECAM antibody. The arrow indicates a blood clot found in this section. The absence of nucleated blood cells and PECAM1-positive endothelial cells around the clot indicates that the clot had a maternal origin. Bars, 500 μm (C, D, and E), 300 μm (F), and 200 μm (G).

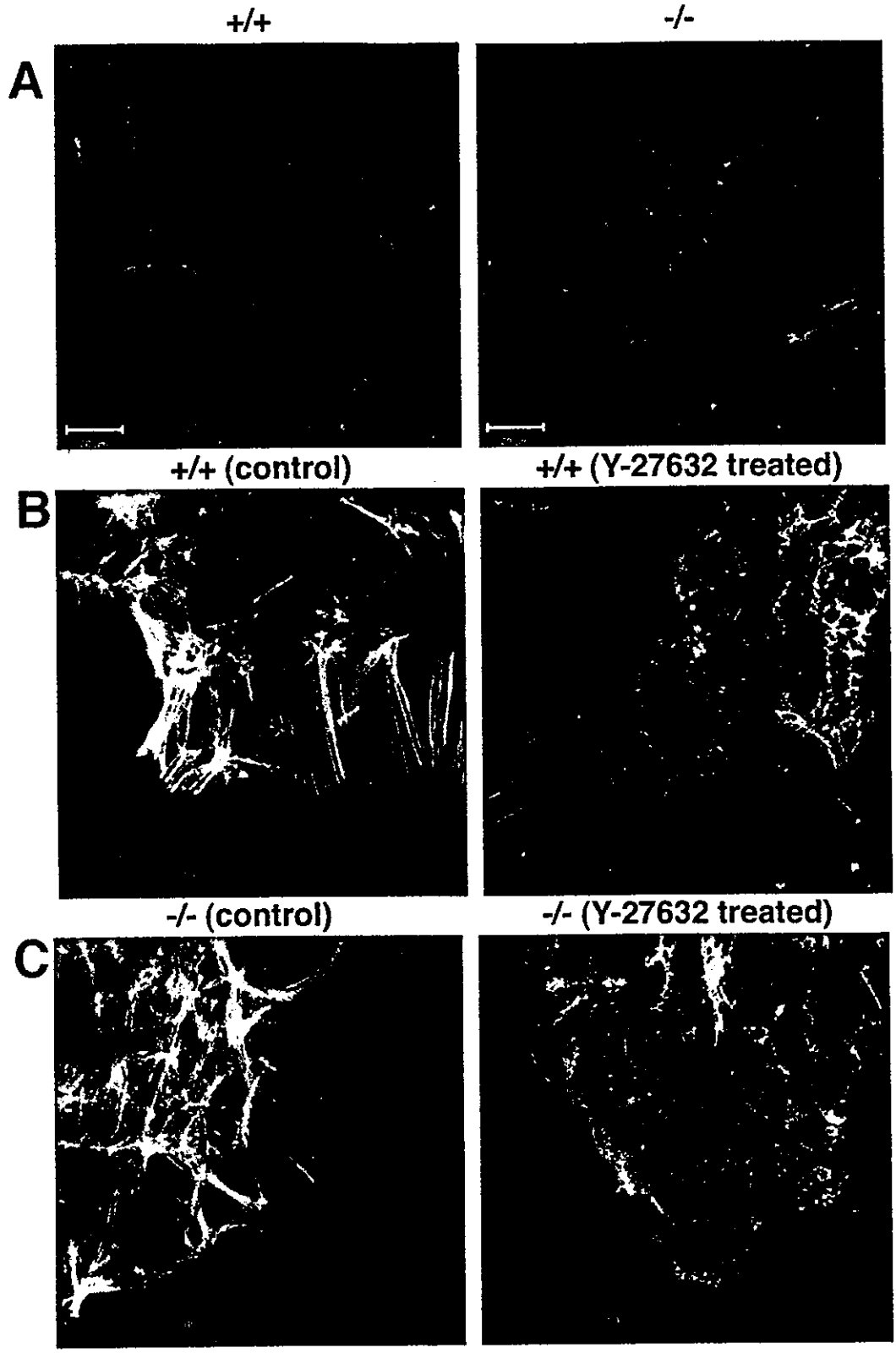

FIG. 6. Architecture of actin fibers in the labyrinth layer and cultured trophoblasts from the placentas of wild-type (ROCK-II$^{+/+}$) and ROCK-II$^{-/-}$ mice. (A) Cytoarchitecture of actin fibers in the labyrinth layer of wild-type and ROCK-II$^{-/-}$ placentas. (B and C) Actin structures in clusters of cultured trophoblasts from wild-type (B) and ROCK-II$^{-/-}$ (C) placentas. Cells were cultured in the absence or presence of 10 μM Y-27632. Note that the structure of actin bundles is not different in the wild-type and ROCK-II$^{-/-}$ cells, and the structures of the actin bundles in the wild-type and ROCK-II$^{-/-}$ cells treated with Y-27632 were similar. Bars, 20 μm (A) and 50 μm (B and C).

TABLE 2. Gene expression change in ROCK-II$^{-/-}$ placenta analyzed by DNA microarray[a]

Gene category and GenBank accession no.	Description	Absolute difference	Fold change
Genes with increased expression in ROCK-II$^{-/-}$ placenta			
AF020525	Prolactin-like protein G precursor	+1,098	+2.3
M35662	Placental lactogen 1	+204	+2.1
M33960	PAI-1	+748	+1.7
Genes with decreased expression in ROCK-II$^{-/-}$ placenta			
AJ007909	Erythroid differentiation regulator	−1,849	−2.9
U58513	mROCK-II	−177	−2.8
Gene with no difference in expression in ROCK-II$^{-/-}$ placenta			
U58512	mROCK-I	+22	1.0

[a] The placenta was excised from 13.5-dpc ROCK-II$^{+/-}$ and ROCK-II$^{-/-}$ embryos of the same litter (two embryos for each group). Gene expression of each ROCK-II$^{-/-}$ placenta was compared with that in two ROCK-II$^{+/-}$ placentas, and genes showing a consistent increase or decrease in four combinations of comparison were chosen. The average differences and changes from four comparisons are shown.

labyrinth layer. However, no significant difference was observed in both the architecture of this network and the strength of actin staining in tissue from wild-type and ROCK-II$^{-/-}$ placentas. Strong actin bundles reminiscent of stress fibers induced by dominant active ROCK (13) were consistently observed in cultured trophoblasts, and there was no difference between ROCK-II$^{+/+}$- and ROCK-II$^{-/-}$-derived trophoblasts cultured on a noncoated cover glass (Fig. 6B and C, left panels) or on a fibronectin-coated cover glass (data not shown). We further found that treatment with 10 μM Y-27632 significantly changed the structure of the actin bundles in the trophoblasts obtained from the labyrinth layers of both wild-type and ROCK-II$^{-/-}$ mice. These results suggest that actin bundles observed in the ROCK-II$^{-/-}$ labyrinth layer and cultured trophoblasts are formed by the action of ROCK-I (Fig. 6B and C, right panels).

Enhanced expression of PAI-1 in the placenta in mROCK-II$^{-/-}$ mice. To investigate the molecular mechanism underlying thrombus formation and placental dysfunction in mROCK-II$^{-/-}$ mice, we next performed DNA microarray analysis to analyze the alterations in gene expression in the absence of ROCK-II. Placentas were isolated from ROCK-II$^{+/-}$ and ROCK-II$^{-/-}$ mice in the same litter at 13.5 dpc and subjected to analysis. We tested about 10,000 genetic loci that have been identified as clusters by the UNIGENE database. Exclusion of expressed sequence tags and genes with low expression (~130 to 180 gene clusters) left only a limited number of genes, whose expression in the placenta of ROCK-II$^{-/-}$ mice was different from that of wild-type mice. Table 2 shows three genes with enhanced expression and two genes with decreased expression in the placenta of ROCK-II$^{-/-}$ mice. The three genes with enhanced expression are the prolactin-like protein G precursor, placental lactogen 1, and PAI-1 genes. One of the two genes showing decreased expression in ROCK-II$^{-/-}$ placentas was mROCK-II itself. Notably, there was no significant difference in mROCK-I expression in ROCK-II$^{-/-}$ and ROCK-II$^{+/-}$ placentas. We further confirmed the elevated expression of PAI-1 by RT-PCR and Northern blotting (Fig. 7). mRNA expression of PAI-1 was significantly higher in all the ROCK-II$^{-/-}$ placentas analyzed (n = 5 for RT-PCR and n = 4 for Northern blotting) than in the heterozygous littermates (Fig. 7). Thus, the loss of ROCK-II resulted in increased expression of PAI-1 in the placenta.

Hemorrhage in the hind limbs of ROCK-II$^{-/-}$ mice. Another feature consistently observed in ROCK-II$^{-/-}$ embryos was hemorrhage in the hind limb bud. Hemorrhage was observed in the tip regions of both hind limb buds in embryos as early as 12.5 dpc, accompanied by swelling of the limb, and persisted until birth (Fig. 3, 4A, 5A and B, and 8A and B). Histological analysis revealed that small capillaries at the tip of the hind limb became significantly dilated at 12.5 dpc and eventually ruptured, causing a hemorrhage at 13.5 dpc (Fig. 8C to E). The bleeding resolved in 3 to 4 days after birth with, in some cases, a deformity left in the feet of adult mice (Fig. 8B). Hemorrhages were also observed in the tip of the tails of ROCK-II$^{-/-}$ embryos but at a lower frequency (2 of 15 dpc 13.5 ROCK-II$^{-/-}$ embryos) (Fig. 8A).

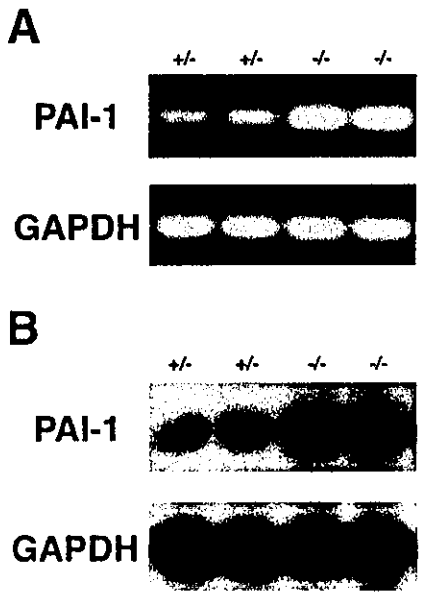

FIG. 7. Elevated expression of PAI-1 in ROCK-II$^{-/-}$ placenta. (A) RT-PCR analysis of PAI-1 expression in ROCK-II$^{+/-}$ and ROCK-II$^{-/-}$ 13.5-dpc placentas. (B) Northern blot analysis of PAI-1 mRNA expression in mROCK-II$^{+/-}$ and mROCK-II$^{-/-}$ 13.5-dpc placentas.

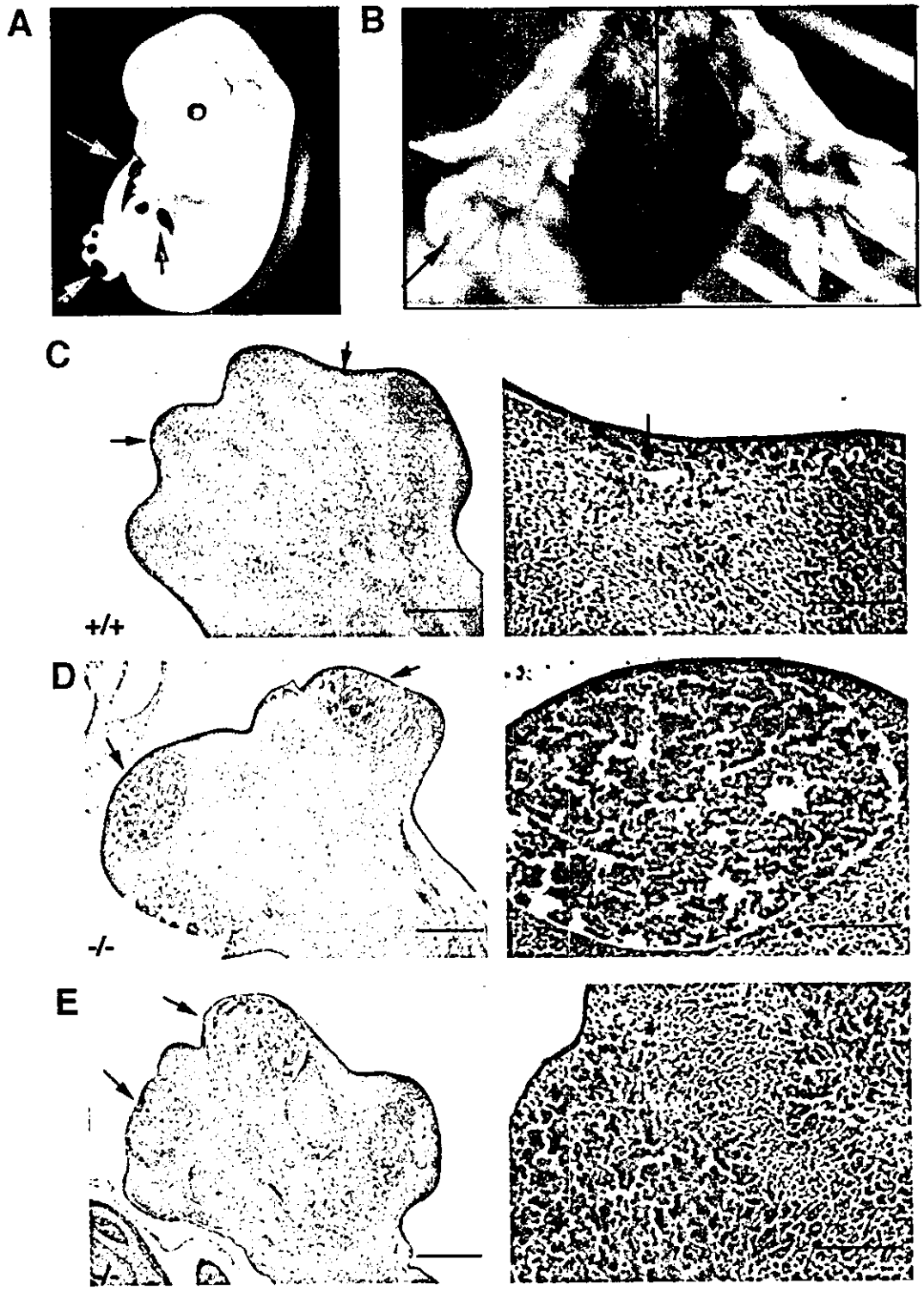

FIG. 8. Hemorrhage in the hind limb of a ROCK-II$^{-/-}$ mouse. (A) Hemorrhage in a 13.5 dpc ROCK-II$^{-/-}$ embryo. Hemorrhages in both hind limbs and at the tip of the tail are indicated by the arrows. (B) Deformity of the hind limb of a ROCK-II$^{-/-}$ mouse. (C to E) Hematoxylin-and-eosin-stained sections of the hind limb bud from a 12.5-dpc wild-type (ROCK-II$^{+/+}$) embryo (C) and 12.5-dpc (D) and 13.5-dpc (E) ROCK-II$^{-/-}$ homozygous embryos. Small capillaries in the hind limbs of wild-type and knockout mice are indicated by the arrows. In panels C, D, and E, lower-magnification (left) and higher-magnification (right) views are shown to the right. Bars, 300 μm (left micrographs of panels C, D, and E) and 100 μm (right micrographs of panels C, D, and E).